

# Fast Penalized Generalized Estimating Equations for Large Longitudinal Functional Datasets

Gabriel Loewinger<sup>1</sup>, Alexander W. Levis<sup>2</sup>, Erjia Cui<sup>3</sup>, Francisco Pereira<sup>1</sup>

<sup>1</sup>Machine Learning Core,  
National Institute of Mental Health

<sup>2</sup>Department of Statistics & Data Science,  
Carnegie Mellon University

<sup>3</sup>Department of Biostatistics and Health Data Science,  
University of Minnesota

## Abstract

Longitudinal binary or count functional data are common in neuroscience, but are often too large to analyze with existing functional regression methods. We propose one-step penalized generalized estimating equations that supports continuous, count, or binary functional outcomes and is fast even when datasets have a large number of clusters and large cluster sizes. The method applies to both functional and scalar covariates, and the one-step estimation framework enables efficient smoothing parameter selection, bootstrapping, and joint confidence interval construction. Importantly, this semi-parametric approach yields coefficient confidence intervals that are provably valid asymptotically even under working correlation misspecification. By developing a general theory for adaptive one-step M-estimation, we prove that the coefficient estimates are asymptotically normal and as efficient as the fully-iterated estimator; we verify these theoretical properties in extensive simulations. Finally, we apply our method to a calcium imaging dataset published in *Nature*, and show that it reveals important timing effects obscured in previous non-functional analyses. In doing so, we demonstrate scaling to common neuroscience dataset sizes: the one-step estimator fits to a dataset with 150,000 (binary) functional outcomes, each observed at 120 functional domain points, in only  $\sim 13.5$  minutes on a laptop without parallelization. We release our implementation in the `fastFGEE` package.

*Keywords:* functional data analysis, longitudinal data analysis, calcium imaging, generalized estimating equations, one-step estimators

# Introduction

Neuroscience studies in animal models provide an invaluable tool to identify the neural mechanisms underpinning brain function and their relationship with psychiatric disorders. Researchers can estimate moment-by-moment associations between experimental covariates (e.g. behavior) and the activity of hundreds of neurons per animal, with widely-used in vivo brain recording techniques like calcium imaging (Grienberger et al., 2022) and *Neuropixels* (Jun et al., 2017). A neuroscientist might study brain-behavior associations on, for example, a learning task in which an animal learns to press a lever for a food reward. These tasks are often performed over hundreds of experimental replicates called “trials” (longitudinal observations akin to “patient visits”). Each trial might be defined as a five second interval starting at extension of the lever and ending with delivery of the food reward. To test whether, for example, mean neural activity is higher on trials when animals press the lever, a common strategy is to analyze scalar summaries of each trial’s neuronal firing activity. For instance, analysts might calculate a firing rate of neuron  $i$  on trial  $j$  by averaging the response,  $Y_{i,j}(s) \in \{0, 1\}$ , across within-trial timepoints indexed by  $s$ :  $\bar{Y}_{i,j} = \frac{1}{|\mathcal{S}|} \sum_{s \in \mathcal{S}} Y_{i,j}(s)$ , where  $\mathcal{S} \subset [0, 5]$  denotes a grid of timepoints at which the outcome is observed. One might then test whether  $\mathbb{E}[\bar{Y}_{i,j} \mid X_{i,j} = 1] - \mathbb{E}[\bar{Y}_{i,j} \mid X_{i,j} = 0] \neq 0$ , where  $X_{i,j}$  is an indicator that the animal on which neuron  $i$  was recorded pressed the lever on trial  $j$ . This analysis approach is parsimonious but discards important temporal information by summarizing across trial timepoints,  $s$ .

Alternatively, the neural response of each five second trial can be conceptualized as a functional outcome, with within-trial timepoints,  $s$ , representing locations along the functional domain. This allows one to apply functional data analysis (FDA, Crainiceanu et al. (2024)) techniques to test how brain-behavior relationships evolve within and across trials (Loewinger et al., 2025). FDA offers a flexible framework to analyze a wide range of neuroscience studies, as it allows both the responses and the covariates (e.g. behavior) to be functional. The size and complexity of our dataset, however, require specialized FDA methods. First, analyses must account for the longitudinal structure, since each neuron’s activity is collected across many trials. Second, the large number of clusters (i.e. neurons) and large cluster sizes (i.e. number of trials recorded for a given neuron), often in the hundreds or thousands, make many longitudinal FDA methods

for binary or count functional outcomes computationally impractical.

To conduct inference in longitudinal FDA with large datasets, we propose a one-step estimator for functional generalized estimating equations (fGEE). Procedurally, we first fit a function-on-scalar regression with a working independence correlation structure to obtain a consistent but potentially inefficient initial estimate of the functional coefficients. We then update the initial estimate with one Newton-Raphson update step, derived from an estimating equation that models intra-cluster correlation. This approach can scale to large datasets and has desirable statistical properties. The initial estimate can be formed quickly because it ignores correlation; using only ‘one step’ in the update is fast because it greatly reduces the number of times potentially large working covariance matrices are inverted. Importantly, our approach still captures much of the statistical efficiency afforded by modeling intra-cluster correlation in longitudinal and/or functional directions with a fully-iterated fGEE. In fact, we prove the one-step fGEE is asymptotically as efficient as the fully-iterated version.

We provide an implementation that supports functional data observed on regular, irregular, dense and sparse grids with functional and/or scalar covariates (see Appendix A.4 for implementation details and Section 7 for links to our Github repos). We further propose adoption of working correlation structures that allow for use of algorithms to efficiently construct and invert large working covariance matrices. We also propose fast strategies for smoothing parameter tuning, cluster bootstrapping, and joint confidence interval construction. We review the literature in Section 1, present our estimator in Section 2, provide theoretical results in Section 3, simulations in Section 4, and a data application in Section 5.

## 1 Related Literature

We focus on the longitudinal function-on-scalar regression literature, where a wide range of conditional and marginal methods have been proposed (Eckardt et al., 2024; Sergazinov et al., 2023; Zhu et al., 2019; Scheipl et al., 2016; Shou et al., 2015; Brockhaus et al., 2015; Scheipl et al., 2015; Zipunnikov et al., 2014; Greven et al., 2011; Morris and Carroll, 2006; Guo, 2002).

Functional mixed models are a versatile conditional strategy for longitudinal FDA. For non-Gaussian functional outcomes, many existing approaches do not scale well to large cluster sizes

or cluster numbers; see discussion and comparison in [Cui et al. \(2022\)](#). [Cui et al. \(2022\)](#); [Loewinger et al. \(2025\)](#); [Zhou et al. \(2025\)](#) proposed a fast functional mixed models approach based on univariate mixed models fits at each functional domain point. These rely on a cluster bootstrap for inference, however, which can be slow for large datasets. Moreover, for non-Gaussian outcomes these approaches yield coefficient estimates that are only interpretable as conditional on the random effects. In many applications, estimates with marginal interpretations are desirable.

Functional GEE and Quadratic Inference Functions (QIF) are marginal methods for longitudinal function-on-scalar regression. [Qu and Li \(2005\)](#) and [Guha Niyogi and Zhong \(2025\)](#) proposed QIF-based methods applicable to FDA, but, to the best of our understanding, these works focused on a single observation of a functional outcome per subject. [Chen et al. \(2013\)](#) proposed a penalized GEE for longitudinal FDA that serves as part of the inspiration for our work. The method, however, requires inverting an  $n_i L \times n_i L$  matrix at each step of model fitting, where  $n_i$  is the size of cluster  $i$ , and  $L$  is the number of points in the functional domain. [Li et al. \(2022\)](#) proposed a marginal estimator for continuous outcomes, but as we show in simulations, it does not scale to large cluster sizes, and has not been extended to binary or count outcomes. Taken together, marginal approaches for longitudinal functional regression with binary or count outcomes do not scale well, thereby limiting their widespread adoption.

Finally, there is a rich literature on penalized longitudinal marginal models for high dimensional covariates with sparsity; see [Xia and Shojaie \(2024\)](#) and references therein. However, we focus on functional data with low dimensional covariates where we do not encourage sparsity.

## 2 Methods

We begin by introducing notation, adopting that used in [Li et al. \(2022\)](#) where possible. We suppose that we observe the functional outcome  $Y_{i,j}(s)$  at point  $s$  for cluster  $i \in [N] := \{1, \dots, N\}$ , at longitudinal observation (e.g. trial or visit)  $j \in [n_i]$ . We express grids as regular (i.e.  $n_i = n_i(s) \ \forall s \in \{s_1, \dots, s_L\}$ ) and evenly spaced for ease of notation, but our methods also apply to irregular and unevenly spaced grids. We denote  $\mathbf{Y}_i(s) \in \mathbb{R}^{n_i}$  as the functional outcome vector at point  $s$  for cluster  $i$ , concatenating all observations  $Y_{i,j}(s)$  for  $j \in [n_i]$ , and write

$\mathbf{Y}_i = [\mathbf{Y}_i(s_1)^T, \dots, \mathbf{Y}_i(s_L)^T]^T \in \mathbb{R}^{n_i L}$ . We denote covariate vector  $\mathbf{X}_{i,j} \in \mathbb{R}^q$  for cluster  $i$  on observation  $j$ , and  $\mathbf{X}_i = [\mathbf{X}_{i,1}, \dots, \mathbf{X}_{i,n_i}]^T \in \mathbb{R}^{n_i \times q}$ . We write covariates as scalar for ease of notation, though our method and theory applies to functional covariates.

## 2.1 Functional Generalized Estimating Equations

We consider the marginal function-on-scalar regression

$$g(\mathbb{E}[Y_{i,j}(s) | \mathbf{X}_{i,j}]) = \eta_{i,j}(s), \quad \eta_{i,j}(s) = \beta_0(s) + \sum_{r=1}^q X_{i,j,r} \beta_r(s), \quad \text{Cov}(\mathbf{Y}_i | \mathbf{X}_i) = \mathbb{V}_i^* \quad (1)$$

where  $g$  is a link function and  $\beta_r(\cdot)$  is a (smooth) coefficient function for covariate  $r \in [q]$ . We let  $\mu_{i,j}(s) = g^{-1}(\eta_{i,j}(s))$  denote the mean function. We now discuss estimation of  $\mu_{i,j}(s)$  with spline basis expansions of the  $\beta_r(\cdot)$ , although our methods can be used for other basis functions. For example, denoting  $\mathbf{B}(s) = [B_1(s), \dots, B_m(s)]^T \in \mathbb{R}^m$  as a set of  $m$  B-spline basis functions, we can represent the functional coefficients  $\beta_r(s) = \sum_{d=1}^m \theta_{r,d} B_d(s)$ . We denote  $\boldsymbol{\theta}_r = [\theta_{r,1}, \dots, \theta_{r,m}]^T \in \mathbb{R}^m$  as an unknown parameter vector associated with covariate  $r$ ,  $\mathbf{B} = [\mathbf{B}(s_1), \dots, \mathbf{B}(s_L)]^T \in \mathbb{R}^{L \times m}$ , and the linear predictor for a full observation of the functional outcome as  $\boldsymbol{\eta}_{i,j} = [\eta_{i,j}(s_1), \dots, \eta_{i,j}(s_L)]^T = \mathbf{B} \boldsymbol{\theta}_0 + \sum_{r=1}^q X_{i,j,r} \mathbf{B} \boldsymbol{\theta}_r$ . We further define  $\mathbb{X}_{i,j} = [\mathbf{B}, X_{i,j,1} \mathbf{B}, \dots, X_{i,j,q} \mathbf{B}] \in \mathbb{R}^{L \times p}$ , where  $p = m(1 + q)$ . We then have that  $\boldsymbol{\eta}_{i,j} = \mathbb{X}_{i,j} \boldsymbol{\theta}$ , where  $\boldsymbol{\theta} = [\boldsymbol{\theta}_0^T, \boldsymbol{\theta}_1^T, \dots, \boldsymbol{\theta}_q^T]^T \in \mathbb{R}^p$ . Thus, we can estimate the functional coefficient vector,  $\boldsymbol{\beta}_r = [\beta_r(s_1), \dots, \beta_r(s_L)]^T \in \mathbb{R}^L$ , by estimating  $\boldsymbol{\theta}$  and calculating  $\hat{\boldsymbol{\beta}}_r = \mathbf{B} \hat{\boldsymbol{\theta}}_r$ .

We semi-parametrically estimate the  $\boldsymbol{\theta}$  with the penalized spline-based fGEE proposed in [Chen et al. \(2013\)](#). This assumes no likelihood and, if  $\mu_{i,j}(s)$  is correctly specified, yields valid inference for  $\{\boldsymbol{\beta}_r(s)\}_{s,r}$  even if  $\text{Cov}(\mathbf{Y}_i | \mathbf{X}_i)$  is misspecified. Specifically, the mean model parameters  $\boldsymbol{\theta}$  are estimated as the root of the penalized estimating equation

$$\sum_{i=1}^N \mathbf{U}_\Lambda(\mathbf{X}_i, \mathbf{Y}_i; \boldsymbol{\theta}_\Lambda) := \sum_{i=1}^N \mathbb{D}_i^T \mathbb{V}_i^{-1} (\mathbf{Y}_i - \boldsymbol{\mu}_i) - \Lambda \mathbb{S} \boldsymbol{\theta}_\Lambda, \quad (2)$$

where  $\mathbb{V}_i \in \mathbb{R}^{n_i L \times n_i L}$  is the working covariance matrix for cluster  $i$  (whose true covariance matrix is  $\mathbb{V}_i^*$ ),  $\mathbb{D}_i = \frac{\partial \boldsymbol{\mu}_i(\boldsymbol{\theta})}{\partial \boldsymbol{\theta}}$ ,  $\mathbb{X}_i = [\mathbb{X}_{i,1}^T, \dots, \mathbb{X}_{i,n_i}^T]^T \in \mathbb{R}^{n_i L \times p}$ , and  $\boldsymbol{\mu}_i = [\boldsymbol{\mu}_{i,1}^T, \dots, \boldsymbol{\mu}_{i,n_i}^T]^T \in \mathbb{R}^{n_i L}$ . The pre-specified penalty matrix,  $\mathbb{S} \in \mathbb{R}^{p \times p}$ , is associated with the diagonal matrix of smoothing

parameters  $\Lambda \in \mathbb{R}^{p \times p}$ . Although no likelihood is adopted, the estimating equation (2) can be derived from the score equations from, for example, an exponential dispersion family (Liang and Zeger, 1986); we add the penalty term for improved estimation in finite samples. Compared to a working independence matrix  $\mathbb{V}_i = I_{n_i L}$ , the estimation of  $\boldsymbol{\theta}$  can be made more efficient and accurate by exploiting correlation, in both functional and longitudinal directions, by choosing the working covariance matrix  $\mathbb{V}_i$  to estimate  $\mathbb{V}_i^*$ . Although such choices for  $\mathbb{V}_i$  in this fGEE model yield desirable statistical properties for longitudinal FDA, estimation is computationally intensive: estimating  $\boldsymbol{\theta}$  based on equation (2) requires inversion of the  $n_i L \times n_i L$  covariance matrix  $\mathbb{V}_i$  for each cluster  $i$ , at each step in an optimization procedure.

## 2.2 One-step fGEE

To scale fGEE to large datasets, we propose a one-step estimator of the form

$$\widehat{\boldsymbol{\theta}}_{\Lambda_1}^{(1)} = \widehat{\boldsymbol{\theta}}_{\Lambda_0}^{(0)} - \left[ \widehat{\mathbb{E}} \left( \nabla_{\boldsymbol{\theta}} U_{\Lambda_1}(\mathbf{X}_i, \mathbf{Y}_i; \widehat{\boldsymbol{\theta}}_{\Lambda_0}^{(0)}) \right) \right]^{-1} \frac{1}{N} \sum_{i=1}^N U_{\Lambda_1}(\mathbf{X}_i, \mathbf{Y}_i; \widehat{\boldsymbol{\theta}}_{\Lambda_0}^{(0)}), \quad (3)$$

where  $\widehat{\boldsymbol{\theta}}_{\Lambda_0}^{(0)}$  is an initial estimate fit with smoothing parameters  $\Lambda_0$ . We estimate (3) as

$$\begin{aligned} \widehat{\boldsymbol{\theta}}_{\Lambda_1}^{(1)} = \widehat{\boldsymbol{\theta}}_{\Lambda_0}^{(0)} + & \left[ \frac{1}{N} \sum_{i=1}^N [\mathbb{D}_i(\widehat{\boldsymbol{\theta}}_{\Lambda_0}^{(0)})]^T [\widehat{\mathbb{V}}_i(\widehat{\boldsymbol{\theta}}_{\Lambda_0}^{(0)})]^{-1} [\mathbb{D}_i(\widehat{\boldsymbol{\theta}}_{\Lambda_0}^{(0)})] + \Lambda_1 \mathbb{S} \right]^{-1} \times \\ & \frac{1}{N} \sum_{i=1}^N \left\{ [\mathbb{D}_i(\widehat{\boldsymbol{\theta}}_{\Lambda_0}^{(0)})]^T [\widehat{\mathbb{V}}_i(\widehat{\boldsymbol{\theta}}_{\Lambda_0}^{(0)})]^{-1} [\mathbf{Y}_i - \widehat{\boldsymbol{\mu}}_i(\widehat{\boldsymbol{\theta}}_{\Lambda_0}^{(0)})] - \Lambda_1 \mathbb{S} \widehat{\boldsymbol{\theta}}_{\Lambda_0}^{(0)} \right\}, \end{aligned} \quad (4)$$

where we plug in  $\widehat{\boldsymbol{\theta}}_{\Lambda_0}^{(0)}$  to calculate  $\mathbb{D}_i(\widehat{\boldsymbol{\theta}}_{\Lambda_0}^{(0)})$ ,  $\widehat{\mathbb{V}}_i(\widehat{\boldsymbol{\theta}}_{\Lambda_0}^{(0)})$ , and  $\widehat{\boldsymbol{\mu}}_i(\widehat{\boldsymbol{\theta}}_{\Lambda_0}^{(0)}) = g^{-1}(\mathbb{X}_i \widehat{\boldsymbol{\theta}}_{\Lambda_0}^{(0)})$ , with  $g^{-1}$  applied component-wise. The updated estimate for the functional coefficient of covariate  $r$  is then obtained as  $\widehat{\boldsymbol{\beta}}_{\Lambda_1, r}^{(1)} = \mathbf{B} \widehat{\boldsymbol{\theta}}_{\Lambda_1, r}^{(1)}$ . Any consistent estimator for  $\boldsymbol{\theta}$  can be used for  $\widehat{\boldsymbol{\theta}}_{\Lambda_0}^{(0)}$ ; we use (2) with a working independence correlation structure, i.e., a function-on-scalar regression that ignores within-cluster correlation of outcome values across  $s$  and  $j$ , and uses the same penalty and spline bases as the fGEE. In practice, we estimate  $\widehat{\boldsymbol{\theta}}_{\Lambda_0}^{(0)}$  with the `pffr` function (Scheipl et al., 2015) from the `refund` package (see Appendix A.3 for details). We formalize the necessary consistency properties of  $\widehat{\boldsymbol{\theta}}_{\Lambda_0}^{(0)}$  for the population parameter,  $\boldsymbol{\theta}$  in Section 3.

The one-step can be conceptualized as a de-biasing of, or equivalently a single Newton-Raphson

step from, the initial estimate  $\widehat{\boldsymbol{\theta}}_{\Lambda_0}^{(0)}$ . It is much faster than the fully-iterated fGEE, because it requires inversion of a working covariance matrix only twice per cluster: 1)  $[\widehat{\mathbb{V}}_i(\widehat{\boldsymbol{\theta}}_{\Lambda_0}^{(0)})]^{-1}$  to estimate  $\widehat{\boldsymbol{\theta}}_{\Lambda_1}^{(1)}$ , and 2)  $[\widehat{\mathbb{V}}_i(\widehat{\boldsymbol{\theta}}_{\Lambda_1}^{(1)})]^{-1}$  to estimate  $\widehat{\text{Var}}(\widehat{\boldsymbol{\theta}}_{\Lambda_1}^{(1)})$  (see Section 2.5).

### 2.3 Working Correlations

Although fGEE yields valid inference regardless of the  $\mathbb{V}_i$  structure used (under correct mean model specification), the statistical and computational efficiency of fGEE depends heavily on the  $\mathbb{V}_i$  form adopted. Our one-step estimator is often far faster than the fully-iterated fGEE in [Chen et al. \(2013\)](#) but, if  $n_i L$  is large, it still may not scale. We therefore focus on parametric forms of  $\mathbb{V}_i$  that can be inverted quickly. We show in simulations below that these forms of  $\mathbb{V}_i$  can still yield the gains in statistical efficiency provided by more flexible  $\mathbb{V}_i$  specifications. Our theory and implementation nevertheless apply to a one-step with general forms of  $\mathbb{V}_i$ .

**Parametric Correlation Structures** For scalability, we focus on adoption of a block working covariance matrix:  $\mathbb{V}_i = \text{bdiag}[\mathbb{V}_i(s_1), \dots, \mathbb{V}_i(s_L)]$ , where  $\mathbb{V}_i(s)$  models  $\text{Cov}(\mathbf{Y}_i(s) \mid \mathbf{X}_i) \in \mathbb{R}^{n_i \times n_i}$ .<sup>1</sup> However, when  $n_i$  is large, even calculating  $\mathbb{V}_i(s)^{-1}$  at one point  $s$  is computationally intensive with standard linear algebra routines. Luckily, exchangeable and AR1 working covariance matrices can be inverted efficiently. For example, rewriting  $\mathbb{V}_i(s) = \mathbf{A}_i^{1/2}(s) \mathbf{R}_i(s) \mathbf{A}_i^{1/2}(s)$ , where  $\mathbf{A}_i(s) = \text{diag}(v_{i,1}(s), \dots, v_{i,n_i}(s))$  and  $v_{i,j}(s)$  models  $\text{Var}(Y_{i,j}(s) \mid \mathbf{X}_{i,j}) \in \mathbb{R}$ , the inverse of  $\mathbb{V}_i(s)$  with exchangeable structure has the analytical form ([Lipsitz et al., 2017](#))

$$\mathbb{V}_i(s)^{-1} = \frac{1}{1 - \rho(s)} \mathbf{A}_i(s)^{-1} - \frac{\rho(s)}{(1 - \rho(s))[(1 - \rho(s)) + n_i \rho(s)]} (\mathbf{A}_i(s)^{-1/2} \mathbf{1}_{n_i}) (\mathbf{A}_i(s)^{-1/2} \mathbf{1}_{n_i})^T,$$

where  $\mathbf{1}_{n_i}$  is a vector of ones, and  $\rho(s) \in [-1, 1)$  is the intra-cluster correlation coefficient.

If  $\mathbb{V}_i(s)$  has the AR1 structure  $\text{Cor}(Y_{i,j}(s), Y_{i,j'}(s) \mid \mathbf{X}_{i,j}) = \rho(s)^{|j-j'|}$ ,  $\mathbb{V}_i^{-1}(s)$  can be efficiently computed because, for  $\rho(s) \geq 0$ , its decomposition yields a Toeplitz  $\mathbf{R}_i(s)$ . For an estimated  $\widehat{\mathbf{r}}_i(s) = [\mathbf{Y}_i(s) - \widehat{\boldsymbol{\mu}}_i(s)] \widehat{\mathbf{A}}_i(s)^{-1/2}$ , we can quickly calculate  $\widehat{\mathbb{V}}_i(s)^{-1} \widehat{\mathbf{r}}_i(s)$  by solving the Toeplitz system  $\mathbf{a} = \widehat{\mathbf{R}}_i(s) \widehat{\mathbf{r}}_i(s)$  with, for example, the generalized Schur algorithm ([Ammar and Gragg, 1988](#)). This is done without fully constructing the  $n_i \times n_i$  matrix  $\widehat{\mathbb{V}}_i(s)$ . When data are observed

---

<sup>1</sup>Our implementation also allows for modeling covariance in the functional direction (instead of modeling covariance in the longitudinal direction) by adopting an alternative block diagonal correlation structure that specifies  $\text{Cov}(Y_{i,j}(s), Y_{i,j}(s')) \neq 0$  and  $\text{Cov}(Y_{i,j}(s), Y_{i,j'}(s')) = 0$  for  $(s \neq s' \text{ and } j \neq j')$ .

irregularly, one can use the algorithm proposed in Allévius (2018).

**Correlation parameters** When adopting the block exchangeable or AR1 correlation structures, each  $\mathbb{V}_i(s)$  is a function of a nuisance correlation parameter  $\rho(s)$ . We estimate these at each point  $s$  separately and then optionally smooth over the functional domain to reduce variability. Defining residuals as  $e_{i,j}(s) = \frac{Y_{i,j}(s) - \mu_{i,j}(s)}{\sqrt{v(\mu_{i,j}(s))}}$ , we use the method of moments estimator for the exchangeable structure (Molenberghs et al., 2005):  $\hat{\rho}(s) = \frac{1}{N} \sum_{i=1}^N \frac{1}{n_i(n_i-1)} \sum_{j \leq k} \hat{e}_{i,j}(s) \hat{e}_{i,k}(s)$ , and truncate the  $\hat{\rho}(s)$  at  $1 - \epsilon$  or  $-1 + \epsilon$  if they fall outside the  $(-1, 1)$  range. For an AR1 structure, we estimate each  $\rho_i(s)$  with the Yule-Walker equations (Yule, 1927; Walker, 1931) when the longitudinal observations are sampled at regular time intervals. If sampled irregularly, we estimate  $\rho_i(s)$  with the MLE estimator proposed in Allévius (2018). We then calculate  $\hat{\rho}(s) = \frac{1}{N} \sum_{i=1}^N \hat{\rho}_i(s)$  and truncate the  $\hat{\rho}(s)$  at 0 or  $1 - \epsilon$  if they fall outside the  $[0, 1)$  range. The  $\hat{\rho}(s)$  are calculated twice in our framework: 1) first using  $\hat{\boldsymbol{\theta}}_{\Lambda_0}^{(0)}$  to calculate  $\hat{\mathbb{V}}_i(\hat{\boldsymbol{\theta}}_{\Lambda_0}^{(0)})$  that is plugged into the one-step estimator (3), and 2) second using  $\hat{\boldsymbol{\theta}}_{\Lambda_1}^{(1)}$  to calculate  $\hat{\mathbb{V}}_i(\hat{\boldsymbol{\theta}}_{\Lambda_1}^{(1)})$  that is plugged into the  $\widehat{\text{Var}}(\hat{\boldsymbol{\beta}}_{\Lambda_1}^{(1)})$  estimator (see expression (6)).

## 2.4 Tuning $\Lambda$

To calculate an initial estimate of  $\hat{\boldsymbol{\theta}}_{\Lambda_0}^{(0)}$ , we select the smoothing parameters, denoted as  $\Lambda_0$ , with fast restricted maximum likelihood (Wood, 2011). We found, however, that calculating the one-step estimate with the same  $\Lambda_0$  values (i.e.  $\boldsymbol{\theta}_{\Lambda_0}^{(1)}$ ) tends to produce inaccurate coefficient estimates. Therefore, we propose to tune the smoothing parameters for the one-step, denoted as  $\Lambda_1$ , based on the cross-validated prediction performance of the one-step estimator. In our simulations, K-fold cluster cross-validation (CV) produced one-step estimates with better estimation accuracy than one-step estimates based on smoothing parameters selected with GCV<sup>2</sup> or the bootstrap-based procedure proposed in Chen et al. (2013). We use the negative log-likelihood as a CV fit criteria. We propose the following scalable CV for large datasets.

We define the folds,  $\{\mathcal{K}_1, \dots, \mathcal{K}_K\}$ , as a disjoint partition of cluster index sets (i.e. the held-out cluster indices) where, for  $K \geq 2$ ,  $\mathcal{K}_k \subset [N]$  for each  $k \in [K]$ ,  $\bigcup_k \mathcal{K}_k = [N]$ , and  $\mathcal{K}_{k_1} \cap \mathcal{K}_{k_2} = \emptyset$  for all  $k_1 \neq k_2$ . To scale CV to large datasets, we exploit four features of the problem structure.

---

<sup>2</sup>Restricted Maximum Likelihood cannot be used to select smoothing parameters for fGEE because there is no likelihood to maximize (Chen et al., 2013).



First, each fold's one-step estimate is calculated with pre-computable quantities. For example, rewriting the update as

$$\widehat{\boldsymbol{\theta}}_{\Lambda_1}^{(1)} = \widehat{\boldsymbol{\theta}}_{\Lambda_0}^{(0)} + \left[ \frac{1}{N} \sum_{i=1}^N \mathbb{W}_i(\widehat{\boldsymbol{\theta}}_{\Lambda_0}^{(0)}) + \Lambda_1 \mathbb{S} \right]^{-1} \frac{1}{N} \sum_{i=1}^N \left\{ \mathbf{b}_i(\widehat{\boldsymbol{\theta}}_{\Lambda_0}^{(0)}) - \Lambda_1 \mathbb{S} \widehat{\boldsymbol{\theta}}_{\Lambda_0}^{(0)} \right\},$$

illustrates that we can pre-compute each cluster's  $\mathbb{W}_i(\widehat{\boldsymbol{\theta}}_{\Lambda_0}^{(0)}) = [\mathbb{D}_i(\widehat{\boldsymbol{\theta}}_{\Lambda_0}^{(0)})]^T [\widehat{\mathbb{V}}_i(\widehat{\boldsymbol{\theta}}_{\Lambda_0}^{(0)})]^{-1} [\mathbb{D}_i(\widehat{\boldsymbol{\theta}}_{\Lambda_0}^{(0)})] \in \mathbb{R}^{p \times p}$ , and  $\mathbf{b}_i(\widehat{\boldsymbol{\theta}}_{\Lambda_0}^{(0)}) = [\mathbb{D}_i(\widehat{\boldsymbol{\theta}}_{\Lambda_0}^{(0)})]^T [\widehat{\mathbb{V}}_i(\widehat{\boldsymbol{\theta}}_{\Lambda_0}^{(0)})]^{-1} [\mathbf{Y}_i - \widehat{\boldsymbol{\mu}}_i(\widehat{\boldsymbol{\theta}}_{\Lambda_0}^{(0)})] \in \mathbb{R}^p$ . Second, we only need to estimate  $\widehat{\boldsymbol{\theta}}_{\Lambda_0}^{(0)}$  once. We can then use that  $\widehat{\boldsymbol{\theta}}_{\Lambda_0}^{(0)}$ , calculated on the full sample, as the initial estimate for all folds and  $\Lambda_1$  values. This is because any consistent initial estimate,  $\widehat{\boldsymbol{\theta}}_{\Lambda_0}^{(0)}$ , is sufficient to ensure that the one-step estimator of a given fold is consistent for the population  $\boldsymbol{\theta}$ . This strategy may be unnecessary for datasets where  $K$  fold-specific initial estimates can be calculated quickly. Third, assuming  $\frac{1}{N} \sum_{i=1}^N \mathbb{W}_i(\widehat{\boldsymbol{\theta}}_{\Lambda_0}^{(0)}) + \Lambda_1 \xrightarrow{\mathbb{P}} \mathbb{E}[\nabla_{\boldsymbol{\theta}} \mathbf{U}_{\Lambda_1}(\mathbf{X}_i, \mathbf{Y}_i; \boldsymbol{\theta}_{\Lambda_0})]$ , we can (heuristically, by Slutsky's theorem) calculate consistent one-step estimates in fold  $k$  as

$$\widehat{\boldsymbol{\theta}}_{\Lambda_1}^k = \widehat{\boldsymbol{\theta}}_{\Lambda_0}^{(0)} + \left[ \frac{1}{N} \sum_{i=1}^N \mathbb{W}_i(\widehat{\boldsymbol{\theta}}_{\Lambda_0}^{(0)}) + \Lambda_1 \mathbb{S} \right]^{-1} \frac{1}{N} \sum_{i \notin \mathcal{K}_k} \left\{ \tilde{n}_k \mathbf{b}_i(\widehat{\boldsymbol{\theta}}_{\Lambda_0}^{(0)}) - \Lambda_1 \mathbb{S} \widehat{\boldsymbol{\theta}}_{\Lambda_0}^{(0)} \right\}, \quad (5)$$

where  $\tilde{n}_k = \frac{\sum_{i=1}^N n_i}{\sum_{i \notin \mathcal{K}_k} n_i}$ . By using the full sample estimate  $\left[ \frac{1}{N} \sum_{i=1}^N \mathbb{W}_i(\widehat{\boldsymbol{\theta}}_{\Lambda_0}^{(0)}) + \Lambda_1 \mathbb{S} \right]^{-1}$ , we only need to invert this  $p \times p$  matrix once for each value of  $\Lambda_1$ , instead of inverting a fold-specific  $p \times p$  matrix for each unique  $\{k, \Lambda_1\}$  pair. The strategy of keeping  $\widehat{\boldsymbol{\theta}}_{\Lambda_0}^{(0)}$  and  $\left[ \frac{1}{N} \sum_{i=1}^N \mathbb{W}_i(\widehat{\boldsymbol{\theta}}_{\Lambda_0}^{(0)}) + \Lambda_1 \mathbb{S} \right]^{-1}$  fixed across folds is motivated by an analogous strategy for cluster bootstrapping of unpenalized one-step GEE (see Remark and Theorem 3.3 in [Cheng et al. \(2013\)](#)). Specifically, [Cheng et al. \(2013\)](#) showed that a cluster bootstrap that fixes these two quantities (at the full-sample estimates) across replicates enjoys the same theoretical guarantees asymptotically as an approach that re-estimates these quantities in each replicate-specific sample. In our simulations, our adaptation of this strategy for cluster CV was often dramatically faster than, and performed nearly identically to, a CV strategy that calculates  $\widehat{\boldsymbol{\theta}}_{\Lambda_1}^k$  using the fold-specific estimate  $\left[ \frac{1}{N - |\mathcal{K}_k|} \sum_{i \notin \mathcal{K}_k} \mathbb{W}_i(\widehat{\boldsymbol{\theta}}_{\Lambda_0}^{(0)}) + \left( \frac{\sum_{i \notin \mathcal{K}_k} n_i}{\sum_{i=1}^N n_i} \right) \Lambda_1 \mathbb{S} \right]^{-1}$ . Fourth, we avoid tuning over a large grid of  $\Lambda_1$  values by using a sequential CV procedure (see Appendix [A.1](#) for details). We found these strategies performed well with  $K = 10$  in our simulations and data application.

## 2.5 Coefficient Estimator Variance

### 2.5.1 Sandwich Variance Estimator

We estimate the variance of our one-step estimator using the sandwich form

$$\widehat{\mathbf{V}}_{\Lambda}(\boldsymbol{\theta}) = \frac{1}{N} [\widehat{\mathbf{H}}_{\Lambda}(\boldsymbol{\theta})]^{-1} \widehat{\mathbf{M}}_{\Lambda}(\boldsymbol{\theta}) [\widehat{\mathbf{H}}_{\Lambda}(\boldsymbol{\theta})]^{-1}, \quad (6)$$

where  $\widehat{\mathbf{M}}_{\Lambda}(\boldsymbol{\theta}) = \mathbb{P}_N[\mathbf{U}_{\Lambda}(\mathbf{X}_i, \mathbf{Y}_i; \boldsymbol{\theta}) \mathbf{U}_{\Lambda}(\mathbf{X}_i, \mathbf{Y}_i; \boldsymbol{\theta})^T]$ , and  $\widehat{\mathbf{H}}_{\Lambda}(\boldsymbol{\theta}) = \mathbb{P}_N[\mathbb{D}_i(\boldsymbol{\theta})^T \widehat{\mathbf{V}}_i(\boldsymbol{\theta})^{-1} \mathbb{D}_i(\boldsymbol{\theta})] + \Lambda \mathbf{S}$ , and  $\mathbb{P}_N[f(O_i)] = \frac{1}{N} \sum_{i=1}^N f(O_i)$  denotes the sample average of a given function  $f$ . We estimate  $\widehat{\text{Var}}(\widehat{\boldsymbol{\theta}}_{\Lambda_1}^{(1)})$  via  $\widehat{\mathbf{V}}_{\Lambda_1}(\widehat{\boldsymbol{\theta}}_{\Lambda_1}^{(1)})$ , i.e., by plugging in  $\widehat{\boldsymbol{\theta}}_{\Lambda_1}^{(1)}$ ,  $\widehat{\mathbf{V}}_i(\widehat{\boldsymbol{\theta}}_{\Lambda_1}^{(1)})$ ,  $\widehat{\mathbf{A}}_i(\widehat{\boldsymbol{\theta}}_{\Lambda_1}^{(1)})$ , and  $\Lambda_1$ .

### 2.5.2 Fast Cluster Bootstrap Variance Estimator

Motivated by theory for cluster bootstrapping in non-functional one-step GEE ([Cheng et al., 2013](#)), we propose a fast cluster bootstrap as an alternative method to estimate  $\text{Var}(\widehat{\boldsymbol{\theta}}_{\Lambda_1}^{(1)})$ , or to construct non-parametric bootstrap-based joint CIs. Namely, for bootstrap replicate,  $t$

$$\widehat{\boldsymbol{\theta}}_{\Lambda_1}^t = \widehat{\boldsymbol{\theta}}_{\Lambda_1}^{(0)} + \left[ \frac{1}{N} \sum_{i=1}^N \mathbb{W}_i(\widehat{\boldsymbol{\theta}}_{\Lambda_0}^{(0)}) + \Lambda_1 \mathbf{S} \right]^{-1} \frac{1}{N} \sum_{i \in \mathcal{R}_t} \left\{ \tilde{n}_t \mathbf{b}_i(\widehat{\boldsymbol{\theta}}_{\Lambda_0}^{(0)}) - \Lambda_1 \mathbf{S} \widehat{\boldsymbol{\theta}}_{\Lambda_0}^{(0)} \right\}, \quad (7)$$

where  $\mathcal{R}_t$  is a set of cluster indices of size  $N$ , sampled with replacement, and  $\tilde{n}_t = \frac{\sum_{i=1}^N n_i}{\sum_{i \in \mathcal{R}_t} n_i}$ . We estimate  $\text{Var}_{\text{boot}}(\widehat{\boldsymbol{\theta}}_{\Lambda}^{(1)})$  as the sample covariance matrix of the  $T$  bootstrap replicates. Since equation (7) uses the same initial estimate  $\widehat{\boldsymbol{\theta}}_{\Lambda_0}^{(0)}$  and keeps the matrix  $\left[ \frac{1}{N} \sum_{i=1}^N \mathbb{W}_i(\widehat{\boldsymbol{\theta}}_{\Lambda_0}^{(0)}) + \Lambda_1 \mathbf{S} \right]^{-1}$  fixed for all  $t$ , this bootstrapping procedure typically takes less than a second for moderately sized  $p$ . We show in simulations that coverage is comparable between CIs constructed with sandwich and fast bootstrap variance estimators (see Appendix Table 20).

## 2.6 Confidence Intervals

For fixed basis matrix  $\mathbf{B}$ ,  $\widehat{\text{Var}}(\widehat{\boldsymbol{\beta}}) = \text{blockdiag}(\widehat{\Sigma}_1^{(\beta)}, \dots, \widehat{\Sigma}_q^{(\beta)}) = (\mathbf{I}_q \otimes \mathbf{B}) \widehat{\text{Var}}(\widehat{\boldsymbol{\theta}}_{\Lambda_1}^{(1)}) (\mathbf{I}_q \otimes \mathbf{B})^T$ , where  $(\mathbf{I}_q \otimes \mathbf{B})$  is a block diagonal matrix, with  $\mathbf{B}$  in each block. An asymptotically valid  $(1 - \alpha)$ -level *pointwise* CI is given by  $\widehat{\beta}_r(s) \pm z_{1-\alpha/2} \widehat{\sigma}_r^{(\beta)}(s)$ , where  $\widehat{\sigma}_r^{(\beta)}(s) = \sqrt{\widehat{\Sigma}_r^{(\beta)}(s)}$ , and  $\widehat{\Sigma}_r^{(\beta)}(s) \in \mathbb{R}$  is diagonal entry  $s$  of  $\widehat{\Sigma}_r^{(\beta)}$ .

We adapt parametric and non-parametric bootstrap based strategies described in [Degras \(2017\)](#)

to construct  $(1 - \alpha)$ -level *joint* CIs. Briefly, we calculate these at point  $s$  as  $\widehat{\beta}_r(s) \pm \tilde{q}_{1-\alpha}^{(r)} \hat{\sigma}_r^{(\beta)}(s)$ , where we estimate  $\tilde{q}_{1-\alpha}^{(r)}$  as the  $1 - \alpha$  empirical quantile of statistics calculated on a bootstrap sample,  $\{\tilde{\theta}_r^t\}_{t=1}^T$ , drawn from the sampling distribution of  $\widehat{\theta}_{\Lambda_1}^{(1)}$ . For the parametric approach, we sample  $\tilde{\theta}_r^t \sim N_m(\mathbf{0}, \widehat{\Sigma}_r^{(\theta)})$ , with  $\widehat{\Sigma}_r^{(\theta)}$  denoting the  $m \times m$  submatrix of  $\widehat{\text{Var}}\left(\widehat{\theta}_{\Lambda_1}^{(1)}\right)$  associated with covariate  $r$ . For the non-parametric approach, we calculate  $\tilde{\theta}_r^t$  with our fast cluster bootstrap. We then set  $m_r^t = \max\left(|\tilde{\theta}_r^t| \oslash \text{diag}(\widehat{\Sigma}_r^{(\theta)})\right)$ , where  $\oslash$  denotes element-wise division, and estimate  $\tilde{q}_{1-\alpha}^{(r)}$  as the  $1 - \alpha$  empirical quantile of  $\{m_r^t\}_{t=1}^T$ . Estimating  $\tilde{q}_{1-\alpha}^{(r)}$  based on draws of  $\tilde{\theta}_r^t$ , instead of draws of  $\tilde{\beta}_r^t$ , is much faster as usually  $\dim(\theta_r) \ll \dim(\beta_r)$ . We apply the parametric approach in results shown in the main text, but provide simulation results in Appendix C.4 that show the non-parametric strategy achieves similar joint coverage.

### 3 Theory

For a fixed sequence  $\Lambda_N = \text{diag}(\lambda_{N,1}, \dots, \lambda_{N,p})$  with  $\frac{1}{N} \max_{1 \leq j \leq p} \lambda_{N,p} \rightarrow 0$ , let  $\theta_N$  be the solution to the population estimating equation  $\mathbb{E}\{U_N(\mathbf{X}_i, \mathbf{Y}_i; \theta)\} = \mathbf{0}$ , where  $U_N(\mathbf{X}_i, \mathbf{Y}_i; \theta) = \mathbb{D}_i^T(\theta) \mathbb{V}_i^{-1}(\mathbf{Y}_i - \boldsymbol{\mu}_i(\theta)) - \frac{1}{N} \Lambda_N \mathbb{S} \theta$  has components denoted  $U_{N,j}(\mathbf{X}_i, \mathbf{Y}_i; \theta)$  for  $j \in [p]$ , and let  $\beta_N = (I_q \otimes \mathbf{B}) \theta_N$ . We define  $\mathbf{H}_N(\theta) = \mathbb{E}[\mathbb{D}_i^T(\theta) \mathbb{V}_i^{-1} \mathbb{D}_i(\theta) + \frac{1}{N} \Lambda_N \mathbb{S}]$ , and  $\mathbf{M}_N(\theta) = \mathbb{E}[U_N(\mathbf{X}_i, \mathbf{Y}_i; \theta) U_N(\mathbf{X}_i, \mathbf{Y}_i; \theta)^T]$ . Note that implicit to these definitions, and to the ensuing theory, is that we treat the working covariance matrices  $\mathbb{V}_i$  as fixed or computed with the “true” limiting correlation parameters  $\rho(s)$  throughout. In practice, we can replace these with their estimated counterparts  $\widehat{\mathbb{V}}_i$  under the assumption that  $\widehat{\rho}(s) = \rho(s) + o_{\mathbb{P}}(n^{-1/2})$  for all  $s$ , for some limiting parameters  $\rho(s)$ —see Corollary 1 of [Chen et al. \(2013\)](#).

**Theorem 3.1.** *Suppose that the one-step estimators,  $\widehat{\theta}_{\Lambda_N}^{(1)}$  and  $\widehat{\beta}_{\Lambda_N}^{(1)}$ , are constructed using initial estimate,  $\widehat{\theta}_N^{(0)}$ , and that the following conditions hold:*

- (i) *The inverse link function  $g^{-1}$  is three times continuously differentiable.*
- (ii) *The covariates and outcomes have bounded support, i.e.  $\exists M > 0$  such that  $P[\|\mathbf{Y}_i(s)\| \leq M] = 1$  for all  $s \in \mathcal{S}$ , and  $P[|X_{i,j,r}| < M] = 1$ , for all  $j \in [n_i]$  and  $r \in [q]$ .*
- (iii)  $\exists s, t > 0 : \lambda_{\min}(\mathbf{M}_N(\theta_N)) \geq s, \mathbb{E}(|U_{N,j}(\mathbf{X}_i, \mathbf{Y}_i; \theta) U_{N,k}(\mathbf{X}_i, \mathbf{Y}_i; \theta) U_{N,l}(\mathbf{X}_i, \mathbf{Y}_i; \theta)|) \leq t, \forall n \in \mathbb{N}, \forall j, k, l.$

$$(iv) \mathbf{H}_N(\boldsymbol{\theta}_N) = \text{is invertible}, \mathbb{P} \left[ \mathbb{P}_N \left( \nabla_{\boldsymbol{\theta}} \mathbf{U}_N(\mathbf{X}_i, \mathbf{Y}_i; \boldsymbol{\theta}) \Big|_{\boldsymbol{\theta} = \widehat{\boldsymbol{\theta}}_N^{(0)}} \right) \text{ non-singular} \right] = 1,$$

$$\text{and} \left( \mathbb{P}_N \left[ \nabla_{\boldsymbol{\theta}} \mathbf{U}_N(\mathbf{X}_i, \mathbf{Y}_i; \boldsymbol{\theta}) \Big|_{\boldsymbol{\theta} = \widehat{\boldsymbol{\theta}}_N^{(0)}} \right] \right)^{-1} = O_{\mathbb{P}}(1).$$

$$(v) \mathbf{M}_N(\boldsymbol{\theta}_N) = O(1), \mathbf{H}_N(\boldsymbol{\theta}_N) = O(1) \text{ and } \{\mathbf{H}_N(\boldsymbol{\theta}_N)\}^{-1} = O(1).$$

$$(vi) \sqrt{N} \{\mathbf{M}_N(\boldsymbol{\theta}_N)\}^{-1/2} \mathbf{H}_N(\boldsymbol{\theta}_N) (\widehat{\boldsymbol{\theta}}_N^{(0)} - \boldsymbol{\theta}_N) = O_{\mathbb{P}}(1).$$

Then the one-step estimator satisfies  $\sqrt{N} \{\mathbf{V}_N\}^{-1/2} (\widehat{\boldsymbol{\beta}}_{\Lambda_N}^{(1)} - \boldsymbol{\beta}_N) \xrightarrow{d} \mathcal{N}(\mathbf{0}, I_p)$ , where  $\mathbf{V}_N = (I_q \otimes \mathbf{B}) \{\mathbf{H}_N(\boldsymbol{\theta}_N)\}^{-1} \mathbf{M}_N(\boldsymbol{\theta}_N) \{\mathbf{H}_N(\boldsymbol{\theta}_N)\}^{-1} (I_q \otimes \mathbf{B})^T$ .

Condition (i) is a mild smoothness condition that holds for all standard link functions (e.g. logit, log). Condition (ii) is also standard—we expect it holds across essentially all biomedical settings. Note that it could be replaced by weaker moments conditions on the estimating equation, and its derivatives. Condition (iii) is a sufficient condition for the estimating equation to be asymptotically normal and implies that  $\mathbf{M}_N(\boldsymbol{\theta}_N)$  is invertible for all  $N \in \mathbb{N}$ . Condition (iv) also states that the  $\mathbf{H}_N(\boldsymbol{\theta}_N)$ , and its sample analogue, are invertible for all  $N \in \mathbb{N}$ . Condition (v) should hold when the limiting (unpenalized) estimating equation results in full rank limiting  $\mathbf{M}_N$  and  $\mathbf{H}_N$ . This should hold when the design matrices,  $\mathbb{X}_i$ , are full rank. Finally condition (vi) is a statement about the rate of convergence of the initial estimator. In practice, when the  $\widehat{\boldsymbol{\theta}}_N^{(0)}$  is estimated using a penalized unweighted estimating equation, this implies some conditions on the rates of convergence of the smoothing parameter values,  $\Lambda_{0,N}$  and  $\Lambda_N$ . We provide an expanded discussion of this in Appendix B, where we also develop a more general result for adaptive one-step M-estimation that may be of independent interest.

**Remark 3.2.** *Our result shows that the one-step is asymptotically equivalent to the fully-iterated fGEE. Moreover, our result extends to non-linear link functions, while existing fGEE theory is restricted to the linear case (Chen et al., 2013). In the linear case, the one-step shares the same properties as those characterized in Chen et al. (2013), such as the convergence rates in small knot and large knot regimes in terms of the smoothing parameter,  $\Lambda$ . We provide a lengthier discussion of the convergence rates of the coefficient estimates in terms of the smoothing parameters in Appendix B.*

## 4 Simulations

We conducted simulations to assess 95% CI coverage, coefficient estimate accuracy, and algorithm timing. We report results from  $T = 300$  simulation replicates. We fit function-on-scalar regressions using penalized B-splines with 10 knots per functional coefficient. For both simulations, we set  $s \in \mathcal{S} \subset [0, 1]$ ,  $|\mathcal{S}| = L = 100$ ,  $N \in \{50, 100\}$ , and  $n_i \in \{5, 25, 100\}$ . Denoting  $\hat{\beta}_r^t(s)$  as functional coefficient  $r$  for simulation replicate  $t$  as point  $s$ , we report estimation accuracy as  $\text{RMSE} = \frac{1}{T} \sum_{t=1}^T \left[ \frac{1}{(q+1)|\mathcal{S}|} \sum_{r=0}^q \sum_{s \in \mathcal{S}} \left( \beta_r(s) - \hat{\beta}_r^t(s) \right)^2 \right]^{1/2}$ . Denoting  $\text{pCI}_r^t(s)$  as the pointwise CI for replicate  $t$  for functional coefficient  $r$  at point  $s$ , we report the average empirical pointwise coverage as:  $\frac{1}{T(q+1)|\mathcal{S}|} \sum_{t=1}^T \sum_{r=0}^q \sum_{s \in \mathcal{S}} \mathbb{1}(\beta_r(s) \in \text{pCI}_r^t(s))$ . Denoting the joint CI as  $\text{jCI}_r^t(s)$ , we report empirical joint coverage as:  $\frac{1}{T(q+1)} \sum_{t=1}^T \sum_{r=0}^q \mathbb{1}(\beta_r(s) \in \text{jCI}_r^t(s) \forall s \in \mathcal{S})$ . In simulation 1, we generated continuous data to allow comparison with existing methods and a penalized Generalized Least Squares (GLS), which is similar to the fully-iterated fGEE. We show that the one-step with the pointwise working correlation structure, that we adopted for scalability, yields gains in statistical efficiency, and performs as well or better (in finite samples) than a method that adopts the true correlation structure in both longitudinal and functional directions. In simulation 2, we verify the one-step's performance in a binary outcome setting. We include additional simulations in Appendix Section C.1.

### 4.1 Simulation 1: Gaussian Outcome with Exchangeable Correlation

We first tested one-step performance in a setting where the outcome was simulated to be correlated in both longitudinal and functional directions (i.e.  $\text{Cov}(Y_{i,j}(s_1), Y_{i,j'}(s_2) \mid \mathbf{X}_i) \neq 0$  for  $s_1, s_2 \in \mathcal{S}$  and  $j, j' \in [n_i]$ ). Thus this experiment also tests how the one-step performs when the pointwise longitudinal correlation structure we adopt is misspecified (i.e. it ignores the underlying correlation in the functional direction). Specifically, we simulated the outcome with an exchangeable correlation structure, allowing for comparison with the marginal decomposition (“Marginal”) approach proposed in Li et al. (2022), which models both within- and between-functional observation correlation. To provide a fair comparison with the Marginal approach, we based these synthetic data experiments on their marginal decomposition simulation scheme

and code. We simulated data with the model

$$Y_{i,j}(s) = \beta_0(s) + X_{1,i}\beta_1(s) + X_{2,i,j}\beta_2(s) + W_{i,j}(s) + \epsilon_{i,j}(s) \quad (8)$$

where  $\beta_0(s) = 3 + \sin(\pi s) + \sqrt{2}\cos(3\pi s)$ ,  $\beta_1(s) = 3 + \cos(2\pi s) + \sqrt{2}\cos(3\pi s)$ , and  $\beta_2(s) = \frac{1}{60} [\phi(\frac{s-0.2}{0.12}) + \phi(\frac{s-0.1}{0.072})] - \frac{1}{200}\phi(\frac{s-0.35}{0.12}) - \frac{1}{250}\phi(\frac{s-0.65}{0.062})$ . Based on simulations in Li et al. (2022), we drew  $X_{1,i} \sim N(0, 1)$ , and  $X_{2,i,j} = j + e_{i,j}$ , where  $e_{i,j} \sim N(\alpha e_{i,j-1}, 1)$ , with  $e_{i,0} = 0$ ,  $\alpha = 0.7$ . We set parameters as in Li et al. (2022):  $W_{i,j}(s) = \sum_{k=1}^2 (\xi_{i,k} + \zeta_{i,j,k})\psi_k(s)$  where the orthonormal functions  $\psi_1(s) = 1 \forall s \in \mathcal{S}$  and  $\psi_2(s) = \sqrt{2}\sin(2\pi s)$ ,  $\xi_{i,1} \stackrel{\text{iid}}{\sim} N(0, 3)$ ,  $\xi_{i,2} \stackrel{\text{iid}}{\sim} N(0, 2)$ ,  $\zeta_{i,j,1} \stackrel{\text{iid}}{\sim} N(0, 1.5)$  and  $\zeta_{i,j,2} \stackrel{\text{iid}}{\sim} N(0, 1)$ .  $\epsilon_{i,j}(s) \stackrel{\text{iid}}{\sim} N(0, 1.5)$ . We show results from simulations with different parameters in Appendix C.2.

In addition to the Marginal approach, we compared the one-step to three benchmarks: 1) a penalized GLS with an independence working correlation structure (GLS-Ind), 2) a GLS with an exchangeable correlation structure (GLS-Ex), and 3) the initial function-on-scalar regression (FoSR),  $\hat{\beta}_{\Lambda_0}^{(0)}$ . We constructed CIs with a sandwich variance estimator for all methods, using the corresponding independence or exchangeable  $\mathbb{V}_i$  forms. Benchmark 1) shows how our implementation and tuning scheme performs without exploiting intra-cluster correlation, benchmark 2) shows performance of an estimator similar to a fully-iterated version of the one-step fGEE (using the same exchangeable correlation structure), and benchmark 3) shows the performance of a FoSR that ignores intra-cluster correlation. CIs for the FoSR fit should, however, achieve nominal coverage in this correlated setting, given that we use a sandwich variance estimator. See Appendix Sections A.2 and A.3 for further details on benchmarks 1-3. When analyzing continuous data in practice, the closed-form penalized GLS (e.g. GLS-Ex) is fast to calculate and is thus preferable to the one-step. However, we assess one-step performance in the continuous data setting because the availability of a closed-form estimator allows us to test how our *one-step* fGEE performs relative to a method similar to a *fully-iterated* fGEE.

Table 1 shows that the one-step coefficient accuracy is almost identical to the GLS-Ex, suggesting the one-step performs comparably to a fully-iterated fGEE. Moreover, the one-step performs as well or better than the Marginal estimator in Li et al. (2022). Thus, in these simulations,

modeling  $\text{Cov}(Y_{i,j}(s), Y_{i,j'}(s) \mid \mathbf{X}_i)$  at each point  $s$  across values of  $j, j' \in [n_i]$ , is enough to capture efficiency gains, even though the data were simulated such that  $\text{Cov}(Y_{i,j}(s_1), Y_{i,j'}(s_2) \mid \mathbf{X}_i) \neq 0$ , for  $s_1 \neq s_2$ . Table 2 shows that the pointwise coverage of the one-step is at roughly the nominal levels. In contrast, the Marginal grows highly anti-conservative for large  $n_i$ , a feature acknowledged in Li et al. (2022). GLS-Ind tends to be slightly conservative, while FoSR is slightly anti-conservative at smaller sample sizes. Table 3 shows that the joint CIs<sup>3</sup> are somewhat conservative for every method, although less so for FoSR. Together these simulations provide one example of how the correlation structure adopted here for computational reasons can still yields gains in statistical efficiency, even when compared to methods that model correlation in both longitudinal and functional directions.

These simulations also illustrate the scalability of the one-step. Table 4 shows that the one-step scales well with both  $N$  and  $n_i$ . In contrast, the Marginal approach is too memory-intensive to fit larger datasets and fit-times scale super-linearly as a function of  $N$  and  $n_i$ . Appendix A.1.3 has tables comparing performance of the one-step fit with a  $\Lambda_1$  tuned using the “fast K-fold” and “K-fold” CV strategies. The fast K-fold CV approach yields similar performance, often in a fraction of the time. Tables in Appendix C.3 show that one-step 95% CIs achieve similar coverage, and take similar time to calculate, when constructed with sandwich or fast cluster bootstrap  $\widehat{\text{Var}}\left(\widehat{\beta}_{\Lambda_1}^{(1)}\right)$  estimators. Finally, we show in Appendix C.4 that Joint CIs constructed with parametric and fast non-parametric bootstrap strategies achieve similar coverage. Taken together, our strategies for working correlation matrix inversion, smoothing parameter tuning, bootstrapping, and joint CI construction yield fast and accurate results.

## 4.2 Simulation 2: Binary Outcome with AR1 Correlation

We simulated correlated binary data with the `SimCorMultRes` package (Touloumis, 2016) with functional observations observed on an evenly spaced grid. The mean model was

$$\text{logit}(\mathbb{E}(Y_{i,j}(s) \mid \mathbf{X}_{i,j})) = \beta_0(s) + X_{1,i}\beta_1(s) + X_{2,i,j}\beta_2(s) \quad (9)$$

where  $\beta_0(s) = 1 + \frac{1}{3}\sin(\pi s) + \frac{\sqrt{2}}{3}\cos(3\pi s)$ ,  $\beta_1(s) = 1 + \frac{1}{3}\cos(2\pi s) + \frac{\sqrt{2}}{3}\cos(3\pi s)$ ,  $\beta_2(s) =$

---

<sup>3</sup>The Marginal approach does not provide code for joint CIs.

$N$	$n_i$	One-step	GLS-Ex	GLS-Ind	Marginal
25	5	$0.95 \pm 0.01$	$0.95 \pm 0.01$	$0.99 \pm 0.00$	$0.96 \pm 0.01$
	25	$0.97 \pm 0.01$	$0.97 \pm 0.01$	$1.00 \pm 0.00$	$1.01 \pm 0.01$
	100	$1.00 \pm 0.00$	$1.00 \pm 0.00$	$1.01 \pm 0.00$	$1.02 \pm 0.01$
50	5	$0.94 \pm 0.01$	$0.94 \pm 0.01$	$0.99 \pm 0.00$	$0.95 \pm 0.01$
	25	$0.97 \pm 0.00$	$0.97 \pm 0.00$	$1.00 \pm 0.00$	$0.99 \pm 0.01$
	100	$0.99 \pm 0.00$	$0.99 \pm 0.00$	$1.00 \pm 0.00$	$1.04 \pm 0.01$
100	5	$0.94 \pm 0.01$	$0.94 \pm 0.01$	$0.99 \pm 0.00$	$0.93 \pm 0.01$
	25	$0.97 \pm 0.00$	$0.97 \pm 0.00$	$0.99 \pm 0.00$	$0.98 \pm 0.01$
	100	$0.99 \pm 0.00$	$0.99 \pm 0.00$	$1.00 \pm 0.00$	—

Table 1: Functional Coefficient Estimation Performance (RMSE) of each method relative to the FoSR fit ( $\text{RMSE}/\text{RMSE}_{\text{FoSR}}$ ). Outcomes are simulated as Gaussian with exchangeable correlation. Cells contain the average of 300 replicates  $\pm$  SEM (SEM= 0.00 indicates a value  $< 0.01$ ). We indicate out-of-memory (30Gb) with symbol — .

$N$	$n_i$	One-step	GLS-Ex	GLS-Ind	Marginal	FoSR
25	5	$0.92 \pm 0.00$	$0.96 \pm 0.00$	$0.96 \pm 0.00$	$0.94 \pm 0.00$	$0.90 \pm 0.00$
	25	$0.92 \pm 0.00$	$0.95 \pm 0.00$	$0.96 \pm 0.00$	$0.94 \pm 0.00$	$0.92 \pm 0.00$
	100	$0.94 \pm 0.00$	$0.97 \pm 0.00$	$0.96 \pm 0.00$	$0.71 \pm 0.00$	$0.93 \pm 0.00$
50	5	$0.95 \pm 0.00$	$0.97 \pm 0.00$	$0.97 \pm 0.00$	$0.94 \pm 0.00$	$0.91 \pm 0.00$
	25	$0.95 \pm 0.00$	$0.97 \pm 0.00$	$0.97 \pm 0.00$	$0.95 \pm 0.00$	$0.94 \pm 0.00$
	100	$0.94 \pm 0.00$	$0.96 \pm 0.00$	$0.97 \pm 0.00$	$0.70 \pm 0.00$	$0.93 \pm 0.00$
100	5	$0.96 \pm 0.00$	$0.98 \pm 0.00$	$0.97 \pm 0.00$	$0.95 \pm 0.00$	$0.92 \pm 0.00$
	25	$0.96 \pm 0.00$	$0.98 \pm 0.00$	$0.98 \pm 0.00$	$0.95 \pm 0.00$	$0.94 \pm 0.00$
	100	$0.96 \pm 0.00$	$0.97 \pm 0.00$	$0.98 \pm 0.00$	—	$0.95 \pm 0.00$

Table 2: Pointwise 95% CI coverage. Cells contain the average of 300 replicates  $\pm$  SEM (SEM= 0.00 indicates a value  $< 0.01$ ). We indicate out-of-memory (30Gb) with symbol — .

$N$	$n_i$	One-step	GLS-Ex	GLS-Ind	FoSR
25	5	$0.97 \pm 0.00$	$0.99 \pm 0.00$	$0.98 \pm 0.00$	$0.95 \pm 0.00$
	25	$0.97 \pm 0.00$	$0.98 \pm 0.00$	$0.98 \pm 0.00$	$0.97 \pm 0.00$
	100	$0.98 \pm 0.00$	$0.99 \pm 0.00$	$0.99 \pm 0.00$	$0.97 \pm 0.00$
50	5	$0.98 \pm 0.00$	$0.99 \pm 0.00$	$0.99 \pm 0.00$	$0.94 \pm 0.00$
	25	$0.99 \pm 0.00$	$0.99 \pm 0.00$	$0.99 \pm 0.00$	$0.98 \pm 0.00$
	100	$0.98 \pm 0.00$	$0.99 \pm 0.00$	$0.99 \pm 0.00$	$0.97 \pm 0.00$
100	5	$0.99 \pm 0.00$	$0.99 \pm 0.00$	$0.99 \pm 0.00$	$0.96 \pm 0.00$
	25	$0.99 \pm 0.00$	$0.99 \pm 0.00$	$0.99 \pm 0.00$	$0.98 \pm 0.00$
	100	$0.99 \pm 0.00$	$0.99 \pm 0.00$	$0.99 \pm 0.00$	$0.98 \pm 0.00$

Table 3: Joint 95% CI coverage for Gaussian data simulated with exchangeable correlation. Each cell contains the average of 300 replicates  $\pm$  SEM (SEM= 0.00 indicates a value  $< 0.01$ ).



$N$	$n_i$	One-step	GLS-Ex	GLS-Ind	Marginal	FoSR
25	5	20.66 $\pm$ 0.14	9.05 $\pm$ 0.07	8.05 $\pm$ 0.04	0.49 $\pm$ 0.00	0.16 $\pm$ 0.00
	25	23.24 $\pm$ 0.10	11.98 $\pm$ 0.04	11.99 $\pm$ 0.05	4.85 $\pm$ 0.03	0.27 $\pm$ 0.00
	100	54.87 $\pm$ 0.59	35.85 $\pm$ 0.55	35.03 $\pm$ 0.54	75.15 $\pm$ 1.07	1.17 $\pm$ 0.01
50	5	27.45 $\pm$ 0.18	16.00 $\pm$ 0.13	14.60 $\pm$ 0.11	1.15 $\pm$ 0.01	0.21 $\pm$ 0.00
	25	34.59 $\pm$ 0.14	21.37 $\pm$ 0.10	19.97 $\pm$ 0.13	29.79 $\pm$ 0.27	0.45 $\pm$ 0.00
	100	86.76 $\pm$ 1.05	64.70 $\pm$ 0.51	66.35 $\pm$ 0.63	415.64 $\pm$ 2.57	2.15 $\pm$ 0.01
100	5	39.33 $\pm$ 0.21	27.26 $\pm$ 0.13	26.51 $\pm$ 0.14	3.79 $\pm$ 0.03	0.31 $\pm$ 0.00
	25	73.25 $\pm$ 0.90	54.20 $\pm$ 0.73	51.83 $\pm$ 0.74	233.72 $\pm$ 1.69	1.08 $\pm$ 0.02
	100	146.26 $\pm$ 2.27	102.88 $\pm$ 1.43	87.89 $\pm$ 0.99	—	2.79 $\pm$ 0.01

Table 4: Fit Time  $\pm$  SEM (seconds) of each method. Outcomes are simulated as Gaussian with exchangeable correlation. We indicate out-of-memory (30Gb) with symbol — .

$\frac{5}{3}\phi(\frac{s-0.35}{0.1}) - \frac{5}{3}\phi(\frac{s-0.65}{0.2})$ , and  $\phi(\cdot)$  denotes the standard normal density function. The covariates were drawn as described in Section 4.1. The  $n_i L \times n_i L$  covariance matrix was set as  $\text{Cov}(\mathbf{Y}_i | \mathbf{X}_i) = \text{blockdiag}(\Sigma_i(s_1), \dots, \Sigma_i(s_L))$ , where  $\text{Cov}(\mathbf{Y}_i(s) | \mathbf{X}_i) = \Sigma_i(s) \in \mathbb{R}^{n_i \times n_i}$ . We used the AR1 structure  $\text{Cor}(Y_{i,j}(s), Y_{i,j'} | \mathbf{X}_{i,j}) = \rho^{|j-j'|}$  for  $\rho(s) = \rho \in \{0.25, 0.5, 0.75\}$ .

Table 5 shows that the one-step improves coefficient estimation performance relative to the initial FoSR fit,  $\hat{\beta}_{\Lambda_0}^{(0)}$ , particularly when  $n_i$  and/or  $\rho(s)$  is large. Tables 6 and 7 show our approach improves CI coverage relative to FoSR. The one-step coverage hovers around 0.9 (pointwise) and 0.98 (joint). In contrast, the FoSR CI coverage is poor, particularly when both  $\rho$  and  $n_i$  are large. This is unexpected as we use a sandwich variance estimator to construct FoSR CIs (calculated with an independence working correlation), so we expected that they would achieve nominal coverage. Thus, while fitting a FoSR with working independence and using a sandwich estimator for inference may seem like a fast, viable alternative to fGEE (with a working correlation other than independence), it can yield CIs with poor coverage. Finally, the fit times, shown in Table 8, demonstrate the scalability of the one-step estimator.

## 5 Application

We apply our framework to calcium imaging data to illustrate the benefits of longitudinal FDA in analyzing neural recordings. To motivate our approach, we first describe common analysis strategies. There is a rich methodological literature on analyzing neuronal firing data to, for example, identify spike times (Jewell and Witten, 2018), denoise data (Pnevmatikakis et al.,

$N$	$n_i$	0.25	0.5	0.75
25	5	$1.03 \pm 0.01$	$1.02 \pm 0.01$	$0.98 \pm 0.01$
	25	$1.01 \pm 0.01$	$0.99 \pm 0.01$	$0.91 \pm 0.01$
	100	$0.99 \pm 0.00$	$0.97 \pm 0.00$	$0.91 \pm 0.01$
50	5	$1.02 \pm 0.00$	$1.01 \pm 0.01$	$0.98 \pm 0.01$
	25	$1.00 \pm 0.00$	$0.96 \pm 0.00$	$0.90 \pm 0.01$
	100	$0.98 \pm 0.00$	$0.96 \pm 0.00$	$0.91 \pm 0.01$
100	5	$1.01 \pm 0.00$	$1.00 \pm 0.01$	$0.97 \pm 0.01$
	25	$0.99 \pm 0.00$	$0.97 \pm 0.00$	$0.92 \pm 0.01$
	100	$0.99 \pm 0.00$	$0.97 \pm 0.00$	$0.93 \pm 0.00$

Table 5: Functional Coefficient Estimation Performance (RMSE) relative to the FoSR fit ( $\text{RMSE}_{AR1}/\text{RMSE}_{\text{FoSR}}$ ). Each cell contains the average of 300 replicates  $\pm$  SEM (SEM= 0.00 indicates a value  $< 0.01$ ). Table values below 1.0 indicate the one-step has more accurate coefficient estimates. Outcomes are simulated as binary with AR1 correlation coefficient  $\rho(s) = \rho \in \{0.25, 0.5, 0.75\}$ .

2016), identify network connections (Wang et al., 2025), and model interactions between neurons with dynamical systems (Glaser et al., 2020). These analysis approaches have different goals and we do not review them here due to space constraints. Instead we focus on what we have observed are common strategies among experimentalists for hypothesis testing of covariate-neural activity associations, as they have similar goals to our proposed method. These approaches seem to vary largely in how 1) the target neural population is defined, 2) the longitudinal structure is accounted for, and 3) the trial-level neural time-series are modeled.

Since calcium imaging and electrophysiology record the activity of many neurons, and recordings are collected in several animals, analyses differ in how the target population is defined and the nesting of neurons within animal is modeled. For example, the *neural pseudo-population* strategy, as we refer to it, fits a single model to a dataset that pools neurons across animals (e.g. see Figures 1, 3, and 3 of Willmore et al. (2023); Zhang et al. (2023); Roesch et al. (2009), respectively). This conceptualizes neurons, both within and across animals, as exchangeable given covariates and model parameters. The *animal-specific neural population* strategy, as we refer to it, summarizes the collection of neurons separately in each animal, and then summarizes the animal-specific statistics with a secondary pooled test statistic (e.g. see Figs 2H in (Legaria et al., 2022), Fig 1G, 1I in Inácio et al. (2025)). The animal-level summary is usually a model fit to, or an average of, the activity of all neurons recorded from that animal (e.g. see Figs

$N$	$n_i$	One-step			FoSR		
		0.25	0.5	0.75	0.25	0.5	0.75
25	5	0.89 $\pm$ 0.00	0.89 $\pm$ 0.00	0.88 $\pm$ 0.00	0.94 $\pm$ 0.00	0.90 $\pm$ 0.00	0.84 $\pm$ 0.00
	25	0.89 $\pm$ 0.00	0.89 $\pm$ 0.00	0.89 $\pm$ 0.00	0.92 $\pm$ 0.00	0.87 $\pm$ 0.00	0.75 $\pm$ 0.00
	100	0.90 $\pm$ 0.00	0.90 $\pm$ 0.00	0.90 $\pm$ 0.00	0.91 $\pm$ 0.00	0.85 $\pm$ 0.00	0.72 $\pm$ 0.00
50	5	0.90 $\pm$ 0.00	0.90 $\pm$ 0.00	0.90 $\pm$ 0.00	0.93 $\pm$ 0.00	0.90 $\pm$ 0.00	0.84 $\pm$ 0.00
	25	0.91 $\pm$ 0.00	0.91 $\pm$ 0.00	0.91 $\pm$ 0.00	0.92 $\pm$ 0.00	0.86 $\pm$ 0.00	0.74 $\pm$ 0.00
	100	0.91 $\pm$ 0.00	0.91 $\pm$ 0.00	0.90 $\pm$ 0.00	0.90 $\pm$ 0.00	0.84 $\pm$ 0.00	0.71 $\pm$ 0.00
100	5	0.92 $\pm$ 0.00	0.92 $\pm$ 0.00	0.92 $\pm$ 0.00	0.94 $\pm$ 0.00	0.90 $\pm$ 0.00	0.84 $\pm$ 0.00
	25	0.91 $\pm$ 0.00	0.91 $\pm$ 0.00	0.91 $\pm$ 0.00	0.91 $\pm$ 0.00	0.86 $\pm$ 0.00	0.74 $\pm$ 0.00
	100	0.89 $\pm$ 0.00	0.90 $\pm$ 0.00	0.90 $\pm$ 0.00	0.88 $\pm$ 0.00	0.82 $\pm$ 0.00	0.69 $\pm$ 0.00

Table 6: Functional Coefficient Pointwise 95% CI Coverage comparing FoSR with the one-step. Each cell contains the average of 300 replicates  $\pm$  SEM (SEM= 0.00 indicates a value  $< 0.01$ ). Outcomes are simulated as binary with AR1 correlation coefficient  $\rho(s) = \rho \in \{0.25, 0.5, 0.75\}$ .

$N$	$n_i$	One-step			FoSR		
		0.25	0.5	0.75	0.25	0.5	0.75
25	5	0.97 $\pm$ 0.00	0.97 $\pm$ 0.00	0.97 $\pm$ 0.00	0.99 $\pm$ 0.00	0.98 $\pm$ 0.00	0.95 $\pm$ 0.00
	25	0.98 $\pm$ 0.00	0.97 $\pm$ 0.00	0.97 $\pm$ 0.00	0.99 $\pm$ 0.00	0.97 $\pm$ 0.00	0.90 $\pm$ 0.00
	100	0.98 $\pm$ 0.00	0.98 $\pm$ 0.00	0.97 $\pm$ 0.00	0.98 $\pm$ 0.00	0.96 $\pm$ 0.00	0.88 $\pm$ 0.00
50	5	0.98 $\pm$ 0.00	0.98 $\pm$ 0.00	0.98 $\pm$ 0.00	0.99 $\pm$ 0.00	0.98 $\pm$ 0.00	0.95 $\pm$ 0.00
	25	0.98 $\pm$ 0.00	0.98 $\pm$ 0.00	0.98 $\pm$ 0.00	0.99 $\pm$ 0.00	0.97 $\pm$ 0.00	0.90 $\pm$ 0.00
	100	0.98 $\pm$ 0.00	0.98 $\pm$ 0.00	0.98 $\pm$ 0.00	0.98 $\pm$ 0.00	0.96 $\pm$ 0.00	0.87 $\pm$ 0.00
100	5	0.99 $\pm$ 0.00	0.98 $\pm$ 0.00	0.98 $\pm$ 0.00	0.99 $\pm$ 0.00	0.98 $\pm$ 0.00	0.95 $\pm$ 0.00
	25	0.98 $\pm$ 0.00	0.98 $\pm$ 0.00	0.98 $\pm$ 0.00	0.98 $\pm$ 0.00	0.96 $\pm$ 0.00	0.89 $\pm$ 0.00
	100	0.97 $\pm$ 0.00	0.97 $\pm$ 0.00	0.97 $\pm$ 0.00	0.97 $\pm$ 0.00	0.95 $\pm$ 0.00	0.86 $\pm$ 0.00

Table 7: Functional Coefficient Joint 95% CI Coverage comparing FoSR with the one-step. Each cell contains the average of 300 replicates  $\pm$  SEM (SEM= 0.00 indicates a value  $< 0.01$ ). Outcomes are simulated as binary with AR1 correlation coefficient  $\rho(s) = \rho \in \{0.25, 0.5, 0.75\}$ .

$N$	$n_i$	0.25	0.5	0.75
25	5	20.78 $\pm$ 0.11	19.97 $\pm$ 0.17	19.01 $\pm$ 0.06
	25	26.69 $\pm$ 0.23	25.07 $\pm$ 0.23	23.45 $\pm$ 0.09
	100	49.67 $\pm$ 0.64	67.62 $\pm$ 0.50	46.37 $\pm$ 0.36
50	5	29.64 $\pm$ 0.11	29.27 $\pm$ 0.09	29.34 $\pm$ 0.10
	25	43.93 $\pm$ 0.25	39.98 $\pm$ 0.22	39.71 $\pm$ 0.20
	100	111.59 $\pm$ 1.42	98.36 $\pm$ 1.22	96.62 $\pm$ 1.02
100	5	49.28 $\pm$ 0.12	49.78 $\pm$ 0.17	49.33 $\pm$ 0.13
	25	73.97 $\pm$ 0.52	77.71 $\pm$ 0.70	73.89 $\pm$ 0.47
	100	212.35 $\pm$ 3.29	222.63 $\pm$ 2.92	170.01 $\pm$ 1.48

Table 8: Fit Time  $\pm$ SEM (seconds) for the entire one-step estimation procedure. Outcomes are simulated as binary with AR1 correlation coefficient  $\rho(s) = \rho \in \{0.25, 0.5, 0.75\}$ .

2G in (Legaria et al., 2022)). This ignores uncertainty in the animal-level statistics when estimating a pooled test statistic. A third approach estimates a test statistic on data from each neuron separately and then fits a model to those statistics (e.g. see Figures 1K, 2E-H of Inácio et al. (2025)). The pooled test ignores uncertainty in the neuron-level statistics, and models the neuron-level statistics estimated on data from neurons in the same animal as independent.

Analysis strategies differ in how the longitudinal structure of experiments are modeled. One strategy is to treat the neural responses of cluster  $i$  — however defined — as exchangeable across trials given model parameters (e.g. see Figure 3E of Jeong et al. (2022) for an example from photometry). A second strategy averages the response across trials and analyzes those trial-averaged measures (e.g. see Figure 2 of Coddington et al. (2023)). This discards longitudinal information. A third strategy accounts for the longitudinal structure with random effects Loewinger et al. (2025), yielding conditional estimates in binary outcome settings.

Analyses vary in how the densely-sampled neural time-series of each trial is conceptualized. Arguably, the most common strategy analyzes univariate summaries of the time-series (e.g. a trial firing rate for each neuron  $i$  and trial  $j$ :  $\bar{Y}_{i,j} = \frac{1}{|\mathcal{S}|} \sum_{s \in \mathcal{S}} Y_{i,j}(s)$ ) pooled across animals and/or trials (e.g. see Figures 1, 3, and 3 of Willmore et al. (2023); Zhang et al. (2023); Roesch et al. (2009), respectively). This strategy can obscure behavior–brain associations and substantially change scientific conclusions because it discards timing information about how covariate-outcome relationships evolve across trial timepoints (Loewinger et al., 2025). A second strategy is to retain the time-series structure, but model covariate-neural activity associations as constant across trial timepoints for each neuron. For example, Inácio et al. (2025) has the goal of identifying neurons associated with a particular behavior over time (e.g. see Figures 1-2). To that effect, they fit a Pearson correlation between behavior and neural activity in each cell separately. This is comparable to the linear regression  $\mathbb{E}[\mathbf{Y}_{i,j}(s) \mid x_{i,j}(s)] = \gamma_0^{(i)} + \gamma_1^{(i)} x_{i,j}(s)$  (e.g. see figure 1K in Inácio et al. (2025)). This models the covariate–outcome relationship as constant across trial timepoints. A third strategy proposed in (Loewinger et al., 2025) addresses this by modeling each trial as a functional outcome. They demonstrate this strategy on fiber photometry data, a recording technique that yields a single neural signal per animal. It would be desirable to apply longitudinal FDA strategies to other recording techniques, such as calcium

imaging or electrophysiology data. This has not been done, to our knowledge, and we believe this is primarily due to the fact that those modalities record potentially tens of thousands of signals per animal, and existing approaches may not scale.

To address these limitations, we apply our fGEE on a dataset that pools neurons across animals (akin to the “neural pseudo-population” strategy). This accounts for the 1) longitudinal and 2) functional nature of the response in each cluster (i.e. neuron), and 3) does not discard uncertainty in the animal-specific estimates in providing an overall *neural pseudo population-level* estimate. This implicitly assumes a covariance structure where correlation between neurons within-animal is negligible. In some cases, it may be preferable to apply a fGEE to the neurons in each animal separately (i.e. the *animal-specific neural population* strategy). This would allow for functional coefficients to differ across animals, but necessitates an approach to construct a pooled estimate of animal-level fits that propagates uncertainty.

## 5.1 Application Background

We apply our method on data from a recent *Nature* paper studying the role of pyramidal neurons in the primary somatosensory cortex (S1) in behavior and sensory input (Inácio et al., 2025). This study recorded neuronal activity in five mice, from 155 – 262 (mean  $\pm$  SEM:  $184.4 \pm 22.61$ ) neurons per animal. Recording was done in head-fixed animals, running on a ball that tracked their movement speed. The authors were interested in identifying S1 neurons active during spontaneous movements. They tested whether each S1 neuron was associated with running speed, whisker movement, and whisker sensory input.

## 5.2 Identifying neural activity encoding speed information

The correlation analysis used in the original paper could only test the neural activity–speed association on average within trials. In contrast, an FDA approach can test how this association evolves across trial timepoints. To demonstrate that, we randomly sampled  $N = 500$  neurons (clusters) from the five animals, and identified five second intervals when animals spontaneously began to run. The start of this running burst was considered a “trial” (experimental replicate) initiation as typically analyzed in neuroscience. Thus the functional outcome for neuron  $i$ , on trial  $j$  was a binary timeseries vector across five seconds of neural activity measured at 30Hz

(starting at the beginning of the running bout to 5 sec after running initiation). This results in a functional outcome measured at an evenly spaced grid of  $|\mathcal{S}| = 150$  points. Speed,  $X_{i,j}(s) \in \mathbb{R}$  was defined as a functional covariate and took the same value for all neurons recorded from the same animal. The cluster size was  $n_i = 29$  for all neurons  $i \in [N]$ . We fit the model

$$\text{logit}(\mathbb{E}[Y_{i,j,l}(s) \mid X_{i,j}(s)]) = \beta_0(s) + X_{i,j}(s)\beta_1(s),$$

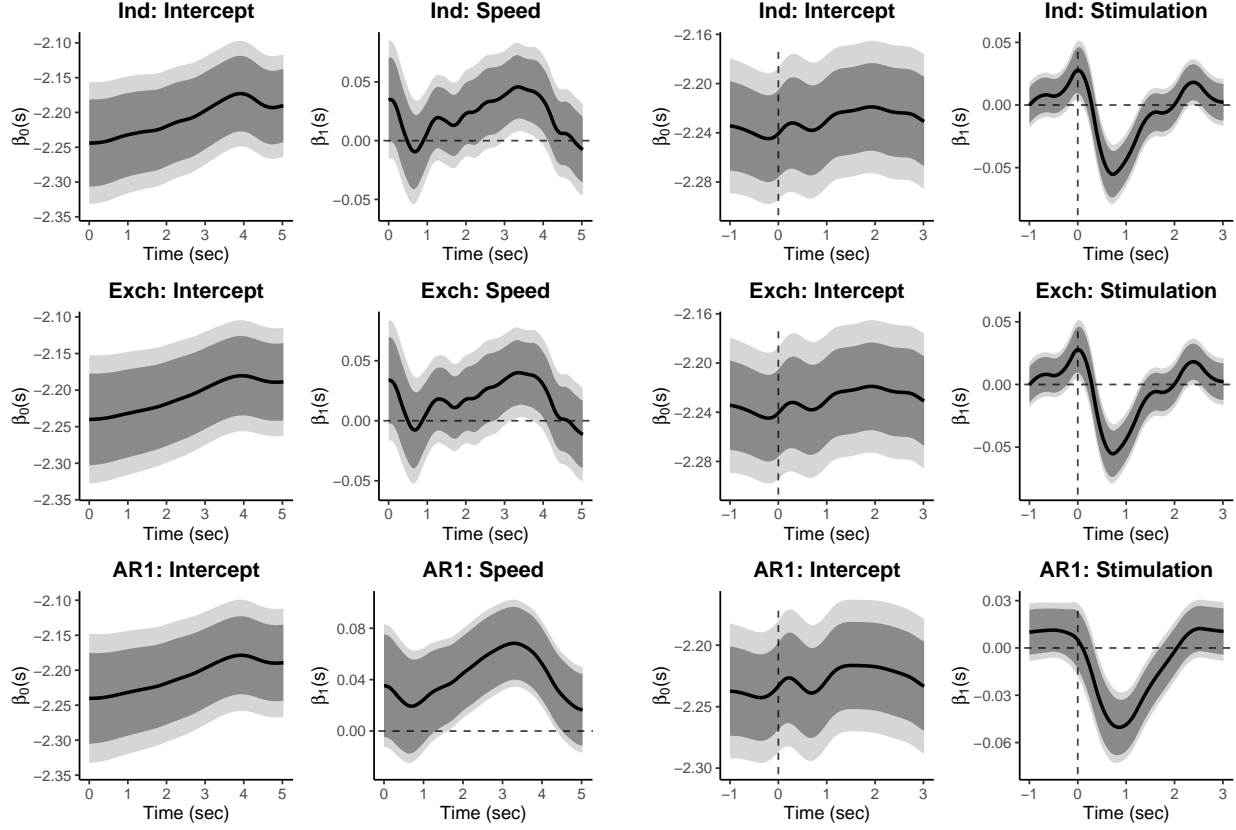
with three possible working correlation structures: independence, exchangeable and AR1. For working independence, we applied the sandwich estimator to the initial FoSR fit,  $\widehat{\beta}_{\Lambda_0}^{(0)}$ .

The independence and exchangeable correlations structures yielded similar results and showed a significant effect only briefly around 3-4 seconds (see Figure 1a). The estimated exchangeable correlation parameter  $\widehat{\rho}(s) \approx 0$  for all  $s$ , and thus the exchangeable and working independence fits were similar. In contrast, the AR1 model showed a much wider time-interval during which effects were significant. This model also had larger  $\widehat{\rho}(s)$  estimates. The AR1 structure is a common correlation structure to adopt in timeseries analysis of neuroscience, and seems more appropriate given that successive trials are recorded close together in time.

The most salient finding was that, even with the AR1 model, the speed–neural activity association does not become significant until about one second after the animals begin to run and that association becomes non-significant fairly quickly. The timing of the association suggests that these neurons are not driving the movement of the animal. This shows how the timing sensitivity of fGEE can help identify the type of cognition or behavior a brain region encodes, which is much harder to do with analyses of trial summary measures.

### 5.3 Whisker Stimulation

The authors of the original paper were also interested in how neural activity in S1 neurons changed as a result of whisker stimulation. The summary analyses they carried out only allowed estimation of the extent to which whisker stimulation changed neural activity on average across within-trial timepoints. To characterize the “temporal dynamics” of the neural response to this manipulation, and demonstrate the scalability of the one-step, we applied our method to activity from  $N = 500$  randomly selected neurons (clusters), each with  $n_i = 300$  observations



(a) Speed–neural activity association.

(b) Whisker stimulation effect.

Figure 1: Functional coefficient estimates for Independent (Ind), Exchangeable (Exch), and Auto-regressive-1 (AR1) working correlation structures.

of the functional outcome: 4 sec of neural activity, measured 1 sec before whisker stimulation to 3 sec after ( $L = 120$ ). We fit the following model

$$\text{logit}(\mathbb{E}[Y_{i,j,l}(s) \mid X_{i,j}]) = \beta_0(s) + X_{i,j}\beta_1(s),$$

where  $X_{i,j} \in \{0, 1\}$  is an indicator that neuron  $i$  was recorded from an animal that was stimulated on trial  $j$ . We fit the model with the same working correlation structures as above.

The one-step estimator, fit to 150,000 functional observations, took  $\sim 13.38$  min to fit on a MacBook Pro with an Apple M1 Max chip with 64GB of RAM, without parallelization, and maintained a reasonable memory footprint throughout. The coefficient associated with stimulation,  $\hat{\beta}_1(s)$ , shows the estimated mean difference in neural activity between stimulated and non-stimulated trials. It appears stimulation leads to a rapid reduction in activity that lasts

about two sec (see Figure 1b). The estimated exchangeable correlation parameter  $\widehat{\rho}(s) = 0$  for all  $s$ , and thus the exchangeable and working independence fits are identical. This analysis illustrates how the one-step makes it possible to identify a clear temporal profile for the effect of interest, and is scalable enough to allow estimation over a large sample of neurons.

In Appendix D, we conduct an additional analysis on this same dataset to examine the association between whisker activity and neural activity. The results reveal that the association between whisker activity and neural activity is significant throughout the trial.

## 6 Discussion

The proposed one-step fGEE can be applied and extended in a range of related settings. For example, only minor adjustments are needed to extend our code to implement an fGEE using a quasi-likelihood based on other distributions (e.g. gamma, beta). In addition to the scalable working covariance forms focused on here, our implementation can also be applied with working covariances,  $\mathbb{V}_i$ , that are estimated more flexibly (e.g. using FPCA). Finally, it should be straightforward to extend our method and code to multivariate functional domains, as well as longitudinal scalar-on-function and function-on-function regressions; we believe parameters from these methods can be estimated through estimating equations with similar forms to the fGEE equations used here. We hope our theoretical guarantees and efficient implementation encourage analysts to apply FDA methods in neuroscience and other settings.

## 7 Software and Reproducibility

Our application and simulation code is in the Github repo: [https://github.com/gloewing/fgee\\_onestep](https://github.com/gloewing/fgee_onestep). The development version of the `fastFGEE` package in R can be found in the Github repo: <https://github.com/gloewing/fastFGEE>.

## Acknowledgments

This research was supported by the Intramural Research Program of the National Institute of Mental Health (NIMH), project ZIC-MH002968. This study utilized the high-performance computational capabilities of the Biowulf Linux cluster at the National Institutes of Health, Bethesda, MD (<http://biowulf.nih.gov>). We thank Dr. Soohyun Lee for allowing us to use her



lab's data in our data application, Dr. Yuan Zhao for advice and help with data pre-processing, Dr. Emily Hector for helpful initial conversations about the method, and Dr. Keith Goldfeld for allowing us to use his package as a starting point for our implementation.

## Appendix A Additional Method Details

### A.1 Cross-Validation Procedure

#### A.1.1 Full-Sample Cross Validation

We define a standard cluster K-Fold Cross-Validation One-Step estimator as

$$\widehat{\boldsymbol{\theta}}_{\Lambda_1}^k = \widehat{\boldsymbol{\theta}}_{\Lambda_0}^{(0)} + \frac{1}{N - |\mathcal{K}_k|} \left[ \frac{1}{N - |\mathcal{K}_k|} \sum_{i \notin \mathcal{K}_k} \mathbb{W}_i(\widehat{\boldsymbol{\theta}}_{\Lambda_0}^{(0)}) + n_k^* \Lambda_1 \mathbb{S} \right]^{-1} \sum_{i \notin \mathcal{K}_k} \left\{ \mathbb{B}_i(\widehat{\boldsymbol{\theta}}_{\Lambda_0}^{(0)}) - n_k^* \Lambda_1 \mathbb{S} \widehat{\boldsymbol{\theta}}_{\Lambda_0}^{(0)} \right\}, \quad (10)$$

where  $n_k^* = \frac{\sum_{i \notin \mathcal{K}_k} n_i}{\sum_{i=1}^N n_i}$ .

#### A.1.2 Sequential Tuning Procedure

The diagonal smoothing matrix  $\Lambda$  contains smoothing parameters  $\lambda_1, \dots, \lambda_q$ , each repeated based on the number of knots used for its functional coefficient. To identify the correct range for the  $\lambda_1, \dots, \lambda_q$ , we apply an iterative CV strategy that is designed to be fast as  $q$  grows. By dividing the tuning into three stages, we avoid tuning over a large  $q$  dimensional grid that can be computationally impractical even for  $q \geq 3$ . In step (1), we tune over a small one-dimensional grid to identify the correct order of magnitude for the smoothing parameters:  $\Lambda_{(1)} = \{\alpha_1 \Lambda^{(0)}, \dots, \alpha_L \Lambda^{(0)}\}$  where, for example,  $\{\alpha_1, \dots, \alpha_{L_1}\} = \{0.001, 0.01, 0.1, 1, 10, 100, 1000\}$ . This exploits the fact that the unique diagonal entries  $\lambda_1^{(0)}, \dots, \lambda_q^{(0)}$  of the  $\Lambda_0$  selected by REML are, in our experience, on a reasonable relative scale. In step (2), we tune over a small  $q$ -dimensional grid constructed around the smoothing parameter values that minimize the cross-validated criteria (e.g. MSE, negative log-likelihood) in step (1). Denoting  $\tilde{\lambda}_1^{(1)}, \dots, \tilde{\lambda}_q^{(1)}$  as these selected values, we tune over a grid with all unique combinations (with the R function `expand.grid()`) of grid  $\Lambda_{(2)} = \left\{ \{\alpha_1 \tilde{\lambda}_1^{(1)}, \dots, \alpha_{L_2} \tilde{\lambda}_1^{(1)}\}, \dots, \{\alpha_1 \tilde{\lambda}_q^{(1)}, \dots, \alpha_L \tilde{\lambda}_q^{(1)}\} \right\}$ , where, for example,  $\{\alpha_1, \dots, \alpha_{L_2}\} = \{0.001, 0.01, 0.1, 1, 10, 100, 1000\}$ . Step (2) identifies a reasonable order of magnitude for each smoothing parameter with a small grid. Finally, in step (3), we tune each smoothing parameter within a local neighborhood around the selected values from step (2),  $\tilde{\lambda}_1^{(2)}, \dots, \tilde{\lambda}_q^{(2)}$ . Specifically,

we tune over the unique combinations,  $\Lambda_{(3)} = \left\{ \{\alpha_1 \tilde{\lambda}_1^{(2)}, \dots, \alpha_{L_3} \tilde{\lambda}_1^{(2)}\}, \dots, \{\alpha_1 \tilde{\lambda}_q^{(2)}, \dots, \alpha_{L_3} \tilde{\lambda}_q^{(2)}\} \right\}$ , where, for example,  $\{\alpha_1, \dots, \alpha_{L_3}\} \subset [0.1, 10]$ . We found this was fast and performed well in simulations for both continuous and binary outcomes, across a wide range of  $N$  and  $n_i$  values. We anticipate the relative speedups of using fast K-fold CV, compared to standard K-fold CV, would be grow as  $p$  increases (e.g. from increasing the number of knots or covariates,  $q$ ). This is because fast K-fold inverts a  $p \times p$  matrix only once per  $\Lambda_1$  value, whereas standard K-fold inverts a similar  $p \times p$  matrix for every unique  $\{k, \Lambda_1\}$  pair.

### A.1.3 Cross-Validation Strategy Performance Comparison

Here we compare performance of the One-Step Estimator trained with the “fast k-fold CV” vs. standard “k-fold CV.” The fast k-fold uses the full-sample matrix  $\left[ \frac{1}{N} \left( \sum_{i=1}^N \nabla_{\boldsymbol{\theta}} \tilde{\mathbf{U}}_{\boldsymbol{\theta}}(\hat{\boldsymbol{\theta}}_{\Lambda_0}^{(0)}) \right) + \Lambda \mathbb{S} \right]^{-1}$  and keeps that fixed across folds, whereas the “k-fold CV” uses  $\left[ \frac{1}{N-|\mathcal{K}_k|} \sum_{i \notin \mathcal{K}_k} \mathbb{W}_i(\hat{\boldsymbol{\theta}}_{\Lambda_0}^{(0)}) + n_k^* \Lambda_1 \mathbb{S} \right]^{-1}$  with the appropriate scaling. We set  $K = 10$ . These results are from the simulation scheme described in main text Section 4.2 “Simulation 2: Gaussian Outcome with Exchangeable Correlation.” Table 9 shows the RMSE of the functional coefficients relative the initial FoSR fit  $\hat{\boldsymbol{\beta}}_{\Lambda_0}^{(0)}$  (fit with `pffr`). The performance of the “fast k-fold CV” is equal or better than that of “k-fold CV.” Table 10 shows the pointwise CI coverage on the One-Step after selecting  $\Lambda_1$  with the two CV procedures. It shows the coverage is indistinguishable. Finally Table 11 shows the runtime, where Fast K-Fold is usually considerably faster (though this depends on  $N$  and  $n_i$ ).

$N$	$n_i$	Fast K-fold	K-fold
25	5	$0.96 \pm 0.00$	$0.96 \pm 0.00$
	25	$0.99 \pm 0.00$	$0.99 \pm 0.00$
	100	$1.01 \pm 0.00$	$1.01 \pm 0.00$
50	5	$0.95 \pm 0.00$	$0.96 \pm 0.00$
	25	$0.98 \pm 0.00$	$0.98 \pm 0.00$
	100	$1.00 \pm 0.00$	$1.01 \pm 0.00$
100	5	$0.95 \pm 0.00$	$0.95 \pm 0.00$
	25	$0.98 \pm 0.00$	$0.98 \pm 0.00$
	100	$0.99 \pm 0.00$	$0.99 \pm 0.00$

Table 9: Comparison of Cross-Validation methods. One-Step Functional Coefficient Estimation Performance (RMSE), tuned with 'Fast K-Fold' or 'K-Fold CV', relative to the initial FoSR fit  $\hat{\beta}_{\Lambda_0}^{(0)}$ : (RMSE/RMSE<sub>FoSR</sub>). Cells contain the average of 300 replicates  $\pm$  SEM (SEM= 0.00 indicates a value  $< 0.01$ ). The results indicate that the "Fast" version of K-Fold CV results in comparable coefficient estimation accuracy to the standard version ( $K = 10$ ).

$N$	$n_i$	Fast K-fold	K-fold
25	5	$0.95 \pm 0.00$	$0.95 \pm 0.00$
	25	$0.95 \pm 0.00$	$0.95 \pm 0.00$
	100	$0.92 \pm 0.00$	$0.92 \pm 0.00$
50	5	$0.96 \pm 0.00$	$0.96 \pm 0.00$
	25	$0.97 \pm 0.00$	$0.97 \pm 0.00$
	100	$0.92 \pm 0.00$	$0.92 \pm 0.00$
100	5	$0.96 \pm 0.00$	$0.96 \pm 0.00$
	25	$0.97 \pm 0.00$	$0.97 \pm 0.00$
	100	$0.97 \pm 0.00$	$0.97 \pm 0.00$

Table 10: Comparison of Cross-Validation methods: Pointwise 95% CI coverage of the final One-Step fit after selecting  $\Lambda_1$  with Fast K-Fold or K-Fold CV.  $K = 10$ . Cells contain the average of 300 replicates  $\pm$  SEM (SEM= 0.00 indicates a value  $< 0.01$ ).

$N$	$n_i$	Fast K-fold	K-fold
25	5	$5.92 \pm 0.16$	$12.32 \pm 0.30$
	25	$8.73 \pm 0.19$	$18.55 \pm 0.44$
	100	$28.77 \pm 0.60$	$44.42 \pm 0.81$
50	5	$9.12 \pm 0.23$	$15.40 \pm 0.37$
	25	$19.12 \pm 0.36$	$26.01 \pm 0.49$
	100	$108.89 \pm 4.01$	$108.86 \pm 3.62$
100	5	$15.56 \pm 0.35$	$22.76 \pm 0.54$
	25	$83.58 \pm 2.54$	$74.23 \pm 2.42$
	100	$93.37 \pm 2.03$	$78.04 \pm 1.67$

Table 11: Comparison of Cross-Validation methods: Entire Fitting Time of Entire One-Step Estimator with Fast K-Fold or K-Fold CV.  $K = 10$ . Cells contain the average of 300 replicates  $\pm$  SEM.

## A.2 Penalized Generalized Least Squares

The penalized Generalized Least Squares (GLS) approach used as a benchmark in the simulations is calculated with the closed-form estimator

$$\hat{\boldsymbol{\theta}}_{\Lambda_G}^{GLS} = \frac{1}{N} \left[ \frac{1}{N} \left( \sum_{i=1}^N \mathbb{X}_i^T [\hat{\mathbb{V}}_i(\hat{\boldsymbol{\theta}}_{\Lambda_0}^{(0)})]^{-1} \mathbb{X}_i \right) + \Lambda_G \mathbb{S} \right]^{-1} \sum_{i=1}^N \mathbb{X}_i^T [\hat{\mathbb{V}}_i(\hat{\boldsymbol{\theta}}_{\Lambda_0}^{(0)})]^{-1} \mathbf{Y}_i \quad (11)$$

where  $\Lambda_0$  is the smoothing parameters selected (with fast restricted maximum likelihood) in the initial fit,  $\hat{\boldsymbol{\theta}}_{\Lambda_0}^{(0)}$ , used in the One-Step estimator. We use the notation  $\Lambda_G$  to denote the smoothing parameters selected based on a GLS-specific fast K-fold cross-validation (CV) procedure. This CV approach is identical to the One-Step fast K-fold CV procedure, except that coefficients are estimated with the above GLS closed-form expression instead of the One-Step estimator. For the exchangeable GLS (*GLS-Ex*), and AR1 GLS (*GLS-AR1*) estimators, we construct  $\mathbb{V}_i$  with the same form as used for the corresponding One-Step  $\mathbb{V}_i$ . For the independent correlation structure GLS (*GLS-Ind*), we set  $\mathbb{V}_i(s) = \mathbf{A}_i^{1/2}(s) \mathbf{R}_i(s) \mathbf{A}_i^{1/2}(s) = \mathbf{A}_i^{1/2}(s) \mathbf{I}_{n_i} \mathbf{A}_i^{1/2}(s) = \mathbf{A}_i(s)$ , where  $\mathbf{A}_i(s) = \text{diag}(v_{i,1}(s), \dots, v_{i,n_i}(s))$  and  $v_{i,j}(s) = \text{Var}(Y_{i,j}(s) \mid \mathbb{X}_{i,j})$ . Otherwise, smoothing parameter tuning, coefficient estimation, and variance calculation is identical to the other GLS estimators.

We estimate  $\text{Var}(\hat{\boldsymbol{\theta}}_{\Lambda_G}^{GLS})$  with the same sandwich estimator as the One-Step

$$\text{Var}(\hat{\boldsymbol{\theta}}_{\Lambda}^{GLS}) = \mathbf{H}_{\Lambda}^{-1} \mathbf{M} \mathbf{H}_{\Lambda}^{-1}, \quad (12)$$

where  $\mathbf{H}_{\Lambda}^{-1} = \sum_{i=1}^N \mathbb{X}_i^T \mathbb{V}_i^{-1} \mathbb{X}_i + \Lambda \mathbb{S}$ , and

$\mathbf{M} = \sum_{i=1}^N \mathbb{X}_i^T \mathbf{A}_i \mathbb{V}_i^{-1} [\mathbf{Y}_i - g^{-1}(\mathbb{X}_i \boldsymbol{\theta})] [\mathbf{Y}_i - g^{-1}(\mathbb{X}_i \boldsymbol{\theta})]^T \mathbb{V}_i^{-1} \mathbf{A}_i \mathbb{X}_i$ , but we instead plug in  $\hat{\boldsymbol{\theta}}_{\Lambda_G}^{GLS}$ ,  $\hat{\mathbb{V}}_i(\hat{\boldsymbol{\theta}}_{\Lambda_G}^{GLS})$ ,  $\hat{\mathbf{A}}_i(\hat{\boldsymbol{\theta}}_{\Lambda_G}^{GLS})$ , and  $\Lambda_G$ . For example, to calculate  $\hat{\mathbb{V}}_i(\hat{\boldsymbol{\theta}}_{\Lambda_G}^{GLS})$ , we estimate the correlation parameters,  $\hat{\rho}(s)$ , using the GLS estimates,  $\hat{\boldsymbol{\theta}}_{\Lambda_G}^{GLS}$ .

### A.3 Initial FoSR pffr fit

As an initial fit, the penalized maximum likelihood estimator

$$\widehat{\boldsymbol{\theta}}_{\Lambda_0}^{(0)} = \underset{\boldsymbol{\theta}}{\operatorname{argmin}} \quad -2 \sum_{i=1}^N \sum_{j=1}^{n_i} \sum_{s \in \mathcal{S}} l(Y_{i,j}(s), \mathbb{X}_{i,j}; \boldsymbol{\theta}) + \boldsymbol{\theta}^T \Lambda_0 \mathbb{S} \boldsymbol{\theta}, \quad (13)$$

where  $l(Y_{i,j}(s), \mathbb{X}_{i,j}; \boldsymbol{\theta})$  is the log-likelihood evaluated on a single observation of the outcome  $Y_{i,j}(s) \in \mathbb{R}$  from cluster  $i$ , at longitudinal observation  $j$ , at functional domain point  $s$ . We denote the model parameter  $\boldsymbol{\theta}$ ,  $\mathbb{S}$  as the penalty matrix, and  $\Lambda_0$  as an associated diagonal matrix of smoothing parameters. As discussed in the main text,  $\mathbb{X}_{i,j} \in \mathbb{R}^p$  is constructed as a product of pre-defined basis functions (e.g. B-splines) and the original covariates,  $\boldsymbol{x}_{i,j} \in \mathbb{R}^q$ . Model 13 is equivalent to adopting a correlation structure that assumes all observations  $Y_{i,j}(s)$  are mutually independent across  $i$ ,  $j$ , and  $s$ .

We fit model 13 with the `refund` package in R (Goldsmith et al., 2024) with the `pffr` function (Scheipl et al., 2015). This calls the `mgcv` package in R (Wood, 2017) to fit the model with the `gam` or `bam` functions. For example, for a model with two covariates, `X1` and `X2`, we use the following code:

```
initial_fit = refund::pffr(Y ~ X1 + X2,
                           family = fam,
                           algorithm = "bam",
                           method = "fREML",
                           discrete = TRUE,
                           bs.yindex = list(bs = spline.basis,
                                              k = knots,
                                              m = m.pffr),
                           data = data_df)
```

where `fam` is the exponential dispersion family adopted to construct a pseudo-likelihood based estimating equation in the fGEE, `spline.basis` is the pre-specified basis spline from the `mgcv` family (e.g. `bs`, `ps`, `tp`), `knots` is the number of knots, and `m.pffr` is the penalty type. For

example, as noted in the `pffr` function, the following

`bs.yindex = list(bs="ps", k=5, m=c(2, 1))` indicates 5 cubic B-splines bases with a first order difference penalty.

## A.4 Computational Details

Our implementation uses a number of R packages for estimation of nuisance parameters and to improve computational speed. We use the `data.table` package extensively to increase computational efficiency (Barrett et al., 2025). Our code structure is loosely based on the structure from the `gee1step` package that implements the One-Step (non-functional) GEE (Lipsitz et al., 2017) available on the Github <https://github.com/kgoldfeld/gee1step> of Professor Keith Goldfeld. We use the `Rfast` package (Papadakis et al., 2018) to estimate the  $\rho(s)$  for AR1 correlation and to speed up other standard computations. We use the `MASS` package to draw multivariate normals (Venables and Ripley, 2002). We use Allévius (2018) to estimate and invert covariance matrices with an AR1 structure when the time intervals are irregular. We use the `SuperGauss` package (Ling and Lysy, 2022) to invert AR1 matrices with regular time intervals. We use the `sanic` package to quickly invert other positive definite matrices (Kuschnig, 2023). As mentioned in the main text and previous Appendix section, we use `mgcv` (Wood, 2017) and `refund` (Goldsmith et al., 2024) packages to estimate initial fits and to (optionally) smooth the correlation parameters across the functional domain.

## Appendix B Theory

Throughout, we fix an arbitrary matrix norm  $\|\cdot\|$  (e.g., operator, Frobenius), and for a sequence of random matrices  $(A_N)_{N=1}^\infty$ , we write  $A_N = O_{\mathbb{P}}(1)$  if  $\|A_N\| = O_{\mathbb{P}}(1)$ , and  $A_N = o_{\mathbb{P}}(1)$  if  $\|A_N\| = o_{\mathbb{P}}(1)$ . For symmetric matrix  $A$ , we write  $\lambda_{\min}(A)$  and  $\lambda_{\max}(A)$  for the smallest and largest eigenvalues of  $A$ , respectively. We begin by stating and proving a lemma that we use to prove our general theorem.

**Lemma B.1.** *Let  $A_N \in \mathbb{R}^{p \times p}$  be a sequence of fixed and invertible matrices such that  $A_N = O(1)$  and  $A_N^{-1} = O(1)$ , let  $X_N \in \mathbb{R}^p$  be a sequence of random vectors such that for constant scalars  $r_N \rightarrow \infty$ ,  $r_N A_N X_N = O_{\mathbb{P}}(1)$ . If  $B_N \in \mathbb{R}^{p \times p}$  is a set of random matrices that satisfy  $B_N \xrightarrow{\mathbb{P}} \mathbf{0}_{p \times p}$ , then  $r_N A_N B_N X_N \xrightarrow{\mathbb{P}} \mathbf{0}_p$ .*

*Proof.* Noting that  $A_N B_N = O(1) o_{\mathbb{P}}(1) = o_{\mathbb{P}}(1)$ , and

$$r_N X_N = A_N^{-1} (r_N A_N X_N) = O(1) O_{\mathbb{P}}(1) = O_{\mathbb{P}}(1)$$

we can immediately conclude that

$$r_N A_N B_N X_N = A_N B_N (r_N X_N) = o_{\mathbb{P}}(1) O_{\mathbb{P}}(1) = o_{\mathbb{P}}(1),$$

as claimed.  $\square$

We now consider a general adaptive  $M$ -estimation setting. Suppose we observe an iid sequence of random vectors  $(Z_i)_{i=1}^{\infty}$ , with generic observation denoted  $Z \sim \mathbb{P}$ , and for each fixed sample size  $N$  we work with the differentiable (in  $\boldsymbol{\theta}$ ) estimating equation  $\boldsymbol{U}_N(Z; \boldsymbol{\theta}) \in \mathbb{R}^p$ , for parameters  $\boldsymbol{\theta} \in \mathbb{R}^p$ . We write  $U_{N,\ell}(Z; \boldsymbol{\theta})$  for the  $\ell$ -th component of  $\boldsymbol{U}_N(Z; \boldsymbol{\theta})$ . The “fully iterated” estimator  $\hat{\boldsymbol{\theta}}_N^*$  would be given by solving

$$\mathbb{P}_N \{ \boldsymbol{U}_N(Z; \boldsymbol{\theta}) \} \equiv \frac{1}{N} \sum_{i=1}^N \boldsymbol{U}_N(Z_i; \boldsymbol{\theta}) = \mathbf{0}_p,$$

targeting the population parameter  $\boldsymbol{\theta}_N$  that solves  $\mathbb{E}\{\boldsymbol{U}_N(Z; \boldsymbol{\theta})\} = \mathbf{0}_p$ . In practice, we will apply the general theory to the longitudinal functional setup by taking  $Z_i \equiv (\mathbb{X}_i, \mathbf{Y}_i)$  and  $\boldsymbol{U}_N(Z_i; \boldsymbol{\theta}) = \mathbb{D}_i^T \tilde{\mathbb{V}}_{i,n}^{-1} (\mathbf{Y}_i - g^{-1}(\mathbb{X}_i \boldsymbol{\theta})) - \frac{1}{N} \Lambda_N \mathbb{S} \boldsymbol{\theta}$ . In this special case, so long as  $\Lambda_N \rightarrow \mathbf{0}_{p \times p}$  and  $\tilde{\mathbb{V}}_n^{-1} \rightarrow \mathbb{V}^{-1}$ , we have  $\boldsymbol{U}_N \rightarrow \boldsymbol{U}_{\infty}$  where  $\boldsymbol{U}_{\infty}(Z; \boldsymbol{\theta}) = \mathbb{D}^T \mathbb{V}^{-1} (\mathbf{Y} - g^{-1}(\mathbb{X} \boldsymbol{\theta}))$ , with corresponding parameter  $\boldsymbol{\theta}_{\infty}$  solving  $\mathbb{E}\{\boldsymbol{U}_{\infty}(Z; \boldsymbol{\theta})\} = \mathbf{0}_p$ —note that we do not explicitly require such convergence in our general setup.

We require notation for a number of related important quantities. First, define the variance quantities  $\boldsymbol{H}_N(\boldsymbol{\theta}) = \mathbb{E}\{\nabla_{\boldsymbol{\theta}} \boldsymbol{U}_N(Z; \boldsymbol{\theta})\}$ ,  $\boldsymbol{M}_N(\boldsymbol{\theta}) = \mathbb{E}\{\boldsymbol{U}_N(Z; \boldsymbol{\theta}) \boldsymbol{U}_N(Z; \boldsymbol{\theta})^T\}$ , and

$$\boldsymbol{V}_N(\boldsymbol{\theta}) = \frac{1}{N} \{ \boldsymbol{H}_N(\boldsymbol{\theta}) \}^{-1} \boldsymbol{M}_N(\boldsymbol{\theta}) \{ \boldsymbol{H}_N(\boldsymbol{\theta}) \}^{-1}.$$



Next, for an initial estimator  $\widehat{\boldsymbol{\theta}}_N^{(0)}$ , we define

$$\widehat{\boldsymbol{\theta}}_N^{(1)} := \widehat{\boldsymbol{\theta}}_N^{(0)} - \left( \mathbb{P}_N \left[ \nabla_{\boldsymbol{\theta}} \mathbf{U}_N(Z; \boldsymbol{\theta}) \Big|_{\boldsymbol{\theta} = \widehat{\boldsymbol{\theta}}_N^{(0)}} \right] \right)^{-1} \mathbb{P}_N \left[ \mathbf{U}_N(Z; \widehat{\boldsymbol{\theta}}_N^{(0)}) \right].$$

Under weak conditions, writing  $\{\mathbf{V}_N(\boldsymbol{\theta}_N)\}^{-1/2} = \sqrt{N} \{\mathbf{M}_N(\boldsymbol{\theta}_N)\}^{-1/2} \mathbf{H}_N(\boldsymbol{\theta}_N)$ , we typically have the following asymptotic normality result for the fully iterated estimator:

$$\{\mathbf{V}_N(\boldsymbol{\theta}_N)\}^{-1/2} \left( \widehat{\boldsymbol{\theta}}_N^* - \boldsymbol{\theta}_N \right) \xrightarrow{d} \mathcal{N}(\mathbf{0}_p, I_p).$$

In the following result, we lay out conditions under which the one-step estimator  $\widehat{\boldsymbol{\theta}}_N^{(1)}$  achieves the same convergence properties, i.e., is asymptotically equivalent to  $\widehat{\boldsymbol{\theta}}_N^*$ .

**Theorem B.2.** *Suppose the following conditions hold:*

- (i)  $\mathbf{U}_N(z; \boldsymbol{\theta})$  is twice differentiable in  $\boldsymbol{\theta}$  for all  $z$ , and the second derivative is uniformly bounded:  $\exists C_1 > 0$  such that  $\mathbb{P} \left[ \sup_{\boldsymbol{\theta}} \left| \frac{\partial^2 U_{N,\ell}(Z; \boldsymbol{\theta})}{\partial \theta_j \partial \theta_k} \right| \leq C_1 \right] = 1$ , for all  $j, k, \ell$ .
- (ii) The second and third moments of  $\mathbf{U}_N(Z; \boldsymbol{\theta}_N)$  are uniformly bounded below and above, respectively:  $\exists s, t > 0$  such that  $\lambda_{\min}(\mathbf{M}_N(\boldsymbol{\theta}_N)) \geq s$ , and

$$\mathbb{E}(|U_{N,j}(Z; \boldsymbol{\theta}_N) U_{N,k}(Z; \boldsymbol{\theta}_N) U_{N,\ell}(Z; \boldsymbol{\theta}_N)|) \leq t,$$

for all  $N \in \mathbb{N}$  and all  $j, k, \ell$ .

- (iii)  $\mathbf{H}_N(\boldsymbol{\theta}_N)$  is invertible and  $\mathbb{P} \left[ \mathbb{P}_N \left( \nabla_{\boldsymbol{\theta}} \mathbf{U}_N(Z; \boldsymbol{\theta}) \Big|_{\boldsymbol{\theta} = \widehat{\boldsymbol{\theta}}_N^{(0)}} \right) \text{ is non-singular} \right] = 1$ , for all  $N \in \mathbb{N}$ . Moreover,  $\{\mathbf{H}_N(\boldsymbol{\theta}_N)\}^{-1} = O(1)$  and  $\left( \mathbb{P}_N \left[ \nabla_{\boldsymbol{\theta}} \mathbf{U}_N(Z; \boldsymbol{\theta}) \Big|_{\boldsymbol{\theta} = \widehat{\boldsymbol{\theta}}_N^{(0)}} \right] \right)^{-1} = O_{\mathbb{P}}(1)$ .

- (iv)  $\mathbf{M}_N(\boldsymbol{\theta}_N) = O(1)$  and  $\mathbf{H}_N(\boldsymbol{\theta}_N) = O(1)$ .

- (v)  $\exists C_2 > 0 : \mathbb{E}(\|\nabla_{\boldsymbol{\theta}} \mathbf{U}_N(Z; \boldsymbol{\theta})|_{\boldsymbol{\theta} = \boldsymbol{\theta}_N} - \mathbf{H}_N(\boldsymbol{\theta}_N)\|^2) \leq C_2$ , for all  $N \in \mathbb{N}$ .

- (vi)  $\sqrt{N} \{\mathbf{M}_N(\boldsymbol{\theta}_N)\}^{-1/2} \mathbf{H}_N(\boldsymbol{\theta}_N) \left( \widehat{\boldsymbol{\theta}}_N^{(0)} - \boldsymbol{\theta}_N \right) = O_{\mathbb{P}}(1)$ .

Then the one-step estimator satisfies  $\{\mathbf{V}_N(\boldsymbol{\theta}_N)\}^{-1/2} \left( \widehat{\boldsymbol{\theta}}_N^{(1)} - \boldsymbol{\theta}_N \right) \xrightarrow{d} \mathcal{N}(\mathbf{0}_p, I_p)$ .

*Proof of Theorem B.2.* Writing  $\mathbf{U}_N^{(N)}(\boldsymbol{\theta}) = \mathbb{P}_N[\mathbf{U}_N(Z; \boldsymbol{\theta})]$ , and employing a Taylor expansion of  $\mathbf{U}_N^{(N)}$  at the initial estimator around  $\boldsymbol{\theta}_N$ , we have

$$\mathbf{U}_N^{(N)}(\widehat{\boldsymbol{\theta}}_N^{(0)}) = \mathbf{U}_N^{(N)}(\boldsymbol{\theta}_N) + \nabla_{\boldsymbol{\theta}} \mathbf{U}_N^{(N)}(\boldsymbol{\theta}) \Big|_{\boldsymbol{\theta}=\boldsymbol{\theta}_N} (\widehat{\boldsymbol{\theta}}_N^{(0)} - \boldsymbol{\theta}_N) + \begin{bmatrix} (\widehat{\boldsymbol{\theta}}_N^{(0)} - \boldsymbol{\theta}_N)^T \mathbf{Q}_{N,1}(\widetilde{\boldsymbol{\theta}}_N) (\widehat{\boldsymbol{\theta}}_N^{(0)} - \boldsymbol{\theta}_N) \\ \vdots \\ (\widehat{\boldsymbol{\theta}}_N^{(0)} - \boldsymbol{\theta}_N)^T \mathbf{Q}_{N,p}(\widetilde{\boldsymbol{\theta}}_N) (\widehat{\boldsymbol{\theta}}_N^{(0)} - \boldsymbol{\theta}_N), \end{bmatrix}$$

for some  $\widetilde{\boldsymbol{\theta}}$  on the line segment between  $\widehat{\boldsymbol{\theta}}_N^{(0)}$  and  $\boldsymbol{\theta}_N$ , and where  $\mathbf{Q}_{N,j}(\boldsymbol{\theta}) = \nabla_{\boldsymbol{\theta}}^2 U_{N,j}^{(N)}(\boldsymbol{\theta}) \in \mathbb{R}^{p \times p}$  for each  $j \in [p]$ . By definition of the one-step estimator,

$$\begin{aligned} \widehat{\boldsymbol{\theta}}_N^{(1)} - \boldsymbol{\theta}_N &= (\widehat{\boldsymbol{\theta}}_N^{(0)} - \boldsymbol{\theta}_N) - \left( \mathbb{P}_N \left[ \nabla_{\boldsymbol{\theta}} \mathbf{U}_N(Z; \boldsymbol{\theta}) \Big|_{\boldsymbol{\theta}=\widehat{\boldsymbol{\theta}}_N^{(0)}} \right] \right)^{-1} \mathbb{P}_N [\mathbf{U}_N(Z; \widehat{\boldsymbol{\theta}}_N^{(0)})] \\ &= (\widehat{\boldsymbol{\theta}}_N^{(0)} - \boldsymbol{\theta}_N) - \left( \nabla_{\boldsymbol{\theta}} \mathbf{U}_N^{(N)}(\boldsymbol{\theta}) \Big|_{\boldsymbol{\theta}=\widehat{\boldsymbol{\theta}}_N^{(0)}} \right)^{-1} \mathbf{U}_N^{(N)}(\widehat{\boldsymbol{\theta}}_N^{(0)}), \end{aligned}$$

so the Taylor expansion implies

$$\begin{aligned} \widehat{\boldsymbol{\theta}}_N^{(1)} - \boldsymbol{\theta}_N &= - \left( \nabla_{\boldsymbol{\theta}} \mathbf{U}_N^{(N)}(\boldsymbol{\theta}) \Big|_{\boldsymbol{\theta}=\widehat{\boldsymbol{\theta}}_N^{(0)}} \right)^{-1} \mathbf{U}_N^{(N)}(\boldsymbol{\theta}_N) + \left\{ I_p - \left( \nabla_{\boldsymbol{\theta}} \mathbf{U}_N^{(N)}(\boldsymbol{\theta}) \Big|_{\boldsymbol{\theta}=\widehat{\boldsymbol{\theta}}_N^{(0)}} \right)^{-1} \nabla_{\boldsymbol{\theta}} \mathbf{U}_N^{(N)}(\boldsymbol{\theta}) \Big|_{\boldsymbol{\theta}=\boldsymbol{\theta}_N} \right. \\ &\quad \left. - \left( \nabla_{\boldsymbol{\theta}} \mathbf{U}_N^{(N)}(\boldsymbol{\theta}) \Big|_{\boldsymbol{\theta}=\widehat{\boldsymbol{\theta}}_N^{(0)}} \right)^{-1} \begin{bmatrix} (\widehat{\boldsymbol{\theta}}_N^{(0)} - \boldsymbol{\theta}_N)^T \mathbf{Q}_{N,1}(\widetilde{\boldsymbol{\theta}}_N) \\ \vdots \\ (\widehat{\boldsymbol{\theta}}_N^{(0)} - \boldsymbol{\theta}_N)^T \mathbf{Q}_{N,p}(\widetilde{\boldsymbol{\theta}}_N) \end{bmatrix} \right\} (\widehat{\boldsymbol{\theta}}_N^{(0)} - \boldsymbol{\theta}_N). \end{aligned}$$

Multiplying through by  $\{\mathbf{V}_N(\boldsymbol{\theta}_N)\}^{-1/2}$ , we obtain

$$\begin{aligned}
& \{\mathbf{V}_N(\boldsymbol{\theta}_N)\}^{-1/2}(\widehat{\boldsymbol{\theta}}_N^{(1)} - \boldsymbol{\theta}_N) = -\sqrt{N}\{\mathbf{M}_N(\boldsymbol{\theta}_N)\}^{-1/2} \mathbf{H}_N(\boldsymbol{\theta}_N) \overbrace{\left( \nabla_{\boldsymbol{\theta}} \mathbf{U}_N^{(N)}(\boldsymbol{\theta}) \Big|_{\boldsymbol{\theta}=\widehat{\boldsymbol{\theta}}_N^{(0)}} \right)^{-1}}^{\xrightarrow{\mathbb{P}} I_p \text{ by (a)}} \mathbf{U}_N^{(N)}(\boldsymbol{\theta}_N) \\
& + \sqrt{N}\{\mathbf{M}_N(\boldsymbol{\theta}_N)\}^{-1/2} \mathbf{H}_N(\boldsymbol{\theta}_N) \underbrace{\left\{ I_p - \left( \nabla_{\boldsymbol{\theta}} \mathbf{U}_N^{(N)}(\boldsymbol{\theta}) \Big|_{\boldsymbol{\theta}=\widehat{\boldsymbol{\theta}}_N^{(0)}} \right)^{-1} \nabla_{\boldsymbol{\theta}} \mathbf{U}_N^{(N)}(\boldsymbol{\theta}) \Big|_{\boldsymbol{\theta}=\boldsymbol{\theta}_N} \right\}}_{\xrightarrow{\mathbb{P}} \mathbf{0}_{p \times p} \text{ by (b)}} \\
& - \underbrace{\left( \nabla_{\boldsymbol{\theta}} \mathbf{U}_N^{(N)}(\boldsymbol{\theta}) \Big|_{\boldsymbol{\theta}=\widehat{\boldsymbol{\theta}}_N^{(0)}} \right)^{-1} \begin{bmatrix} (\widehat{\boldsymbol{\theta}}_N^{(0)} - \boldsymbol{\theta}_N)^T \mathbf{Q}_{N,1}(\widetilde{\boldsymbol{\theta}}_N) \\ \vdots \\ (\widehat{\boldsymbol{\theta}}_N^{(0)} - \boldsymbol{\theta}_N)^T \mathbf{Q}_{N,p}(\widetilde{\boldsymbol{\theta}}_N) \end{bmatrix}}_{=O_{\mathbb{P}}(1) \text{ by (c)}} \Big\} (\widehat{\boldsymbol{\theta}}_N^{(0)} - \boldsymbol{\theta}_N),
\end{aligned}$$

where we invoked facts (a), (b), and (c) verified below. The first summand converges to a normal distribution by Lemma B.1 and the central limit theorem, whose application is justified under condition (ii). The second summand converges to zero in probability, as is seen by combining condition (vi) and another application of Lemma B.1—note that  $\{\mathbf{M}_N(\boldsymbol{\theta}_N)\}^{1/2}$ ,  $\mathbf{H}_N(\boldsymbol{\theta}_N)$ ,  $\{\mathbf{M}_N(\boldsymbol{\theta}_N)\}^{-1/2}$ , and  $\{\mathbf{H}_N(\boldsymbol{\theta}_N)\}^{-1}$  are all  $O_{\mathbb{P}}(1)$  under conditions (ii), (iii) and (iv).

It remains to verify the following facts:

$$\begin{aligned}
& \text{(a) } \mathbf{H}_N(\boldsymbol{\theta}_N) \left( \nabla_{\boldsymbol{\theta}} \mathbf{U}_N^{(N)}(\boldsymbol{\theta}) \Big|_{\boldsymbol{\theta}=\widehat{\boldsymbol{\theta}}_N^{(0)}} \right)^{-1} \xrightarrow{\mathbb{P}} I_p \\
& \text{(b) } \left( \nabla_{\boldsymbol{\theta}} \mathbf{U}_N^{(N)}(\boldsymbol{\theta}) \Big|_{\boldsymbol{\theta}=\widehat{\boldsymbol{\theta}}_N^{(0)}} \right)^{-1} \nabla_{\boldsymbol{\theta}} \mathbf{U}_N^{(N)}(\boldsymbol{\theta}) \Big|_{\boldsymbol{\theta}=\boldsymbol{\theta}_N} \xrightarrow{\mathbb{P}} I_p \\
& \text{(c) } \left( \nabla_{\boldsymbol{\theta}} \mathbf{U}_N^{(N)}(\boldsymbol{\theta}) \Big|_{\boldsymbol{\theta}=\widehat{\boldsymbol{\theta}}_N^{(0)}} \right)^{-1} \begin{bmatrix} (\widehat{\boldsymbol{\theta}}_N^{(0)} - \boldsymbol{\theta}_N)^T \mathbf{Q}_{N,1}(\widetilde{\boldsymbol{\theta}}_N) \\ \vdots \\ (\widehat{\boldsymbol{\theta}}_N^{(0)} - \boldsymbol{\theta}_N)^T \mathbf{Q}_{N,p}(\widetilde{\boldsymbol{\theta}}_N) \end{bmatrix} \xrightarrow{\mathbb{P}} \mathbf{0}_{p \times p}
\end{aligned}$$

Observe first that  $\widehat{\boldsymbol{\theta}}_N^{(0)} - \boldsymbol{\theta}_N = o_{\mathbb{P}}(1)$  under our assumptions: this follows from condition (vi), and the fact that the matrices  $\{\mathbf{M}_N(\boldsymbol{\theta}_N)\}^{1/2}$  and  $\{\mathbf{H}_N(\boldsymbol{\theta}_N)\}^{-1}$  are bounded under conditions

(iii) and (iv). For fact (a), see that

$$\begin{aligned}
& \nabla_{\boldsymbol{\theta}} \mathbf{U}_N^{(N)}(\boldsymbol{\theta}) \Big|_{\boldsymbol{\theta}=\widehat{\boldsymbol{\theta}}_N^{(0)}} - \mathbf{H}_N(\boldsymbol{\theta}_N) \\
&= \mathbb{P}_N \left[ \nabla_{\boldsymbol{\theta}} \mathbf{U}_N(Z; \boldsymbol{\theta}) \Big|_{\boldsymbol{\theta}=\widehat{\boldsymbol{\theta}}_N^{(0)}} \right] - \mathbb{E} \left( \nabla_{\boldsymbol{\theta}} \mathbf{U}_N(Z; \boldsymbol{\theta}) \Big|_{\boldsymbol{\theta}=\boldsymbol{\theta}_N} \right) \\
&= \mathbb{P}_N \left[ \nabla_{\boldsymbol{\theta}} \mathbf{U}_N(Z; \boldsymbol{\theta}) \Big|_{\boldsymbol{\theta}=\widehat{\boldsymbol{\theta}}_N^{(0)}} - \nabla_{\boldsymbol{\theta}} \mathbf{U}_N(Z; \boldsymbol{\theta}) \Big|_{\boldsymbol{\theta}=\boldsymbol{\theta}_N} \right] \\
&\quad + \left\{ \mathbb{P}_N \left[ \nabla_{\boldsymbol{\theta}} \mathbf{U}_N(Z; \boldsymbol{\theta}) \Big|_{\boldsymbol{\theta}=\boldsymbol{\theta}_N} \right] - \mathbb{E} \left( \nabla_{\boldsymbol{\theta}} \mathbf{U}_N(Z; \boldsymbol{\theta}) \Big|_{\boldsymbol{\theta}=\boldsymbol{\theta}_N} \right) \right\}.
\end{aligned}$$

The first summand is bounded above by  $C_1 \|\widehat{\boldsymbol{\theta}}_N^{(0)} - \boldsymbol{\theta}_N\| = o_{\mathbb{P}}(1)$  by condition (i), and the second summand converges to zero by a weak law of large numbers, justified by condition (v). Thus, (a) holds by the continuous mapping theorem—note that all matrices involved are invertible and stochastically bounded under condition (iii). Fact (b) is shown using the same argument as for the first summand analyzed above for fact (a). Finally, fact (c) holds by condition (i) (i.e., the second derivative matrices are uniformly bounded), the fact that  $\widehat{\boldsymbol{\theta}}_N^{(0)} - \boldsymbol{\theta}_N = o_{\mathbb{P}}(1)$ , and condition (iii) (i.e., the left multiplying matrix is  $O_{\mathbb{P}}(1)$ ),  $\square$

## B.1 Condition (vi)

To provide intuition for condition (vi) in the statement of Theorem B.2, we derive an interpretable set of conditions that imply condition (vi) in a special case of our general framework: a non-functional, univariate (i.e.,  $p = q = 1$ ), non-clustered (i.e.,  $n_i = 1 \ \forall i \in [N]$ ) ridge regression that is weighted by the inverse of the working covariance matrix. This setting provides insight for the more general case: (1) the fully-iterated unweighted ridge is analogous to the initial penalized GEE estimator that is also unweighted (i.e., adopts an independence working covariance structure) and fully-iterated; (2) the fully-iterated weighted ridge is analogous to the fully-iterated and weighted (i.e., adopts some non-independence working covariance structure) penalized GEE. In this special case, we show that if the scaled smoothing parameters for the initial estimate satisfy  $\frac{1}{N}\lambda_{0,N} = O(N^{-1/2})$ , and for the weighted estimator satisfy  $\frac{1}{N}\lambda_N = O(N^{-1/2})$ , then condition (vi) holds. That is, if each of these scaled smoothing parameters individually (i.e., no conditions are required jointly on these rates) go to zero fast enough, then  $\sqrt{N}\{\mathbf{M}_N(\boldsymbol{\theta}_N)\}^{-1/2}\mathbf{H}_N(\boldsymbol{\theta}_N)(\widehat{\boldsymbol{\theta}}_N^{(0)} - \boldsymbol{\theta}_N) = O_{\mathbb{P}}(1)$ . Importantly, the smoothing parameter

rates we require are weaker than (i.e., implied by) the rates needed for the theoretical properties described in [Chen et al. \(2013\)](#). For example, even for the small knot setting, [Chen et al. \(2013\)](#) require that  $\lambda = O(N^\gamma)$  for  $\gamma \leq (\tilde{p} + 2 - \tilde{q})/(2\tilde{p} + 3)$ . This implies, for instance, that for a  $\tilde{p}^{th}$  order truncated polynomial using cubic B-splines,  $\gamma \leq (\tilde{p} + 2 - (\tilde{p} + 1))/(2\tilde{p} + 3) = 1/9$ . Put onto the scale of a single cluster, [Chen et al. \(2013\)](#) requires the faster rate of  $\frac{1}{N}\lambda = O(N^{-8/9})$  than the  $O(N^{-1/2})$  rate required by our theory in this special case. By this reasoning, condition (vi) is a weak assumption in this special case. Our conjecture is that this extends to more complicated settings although we omit such analysis in this work.

**Univariate Weighted Ridge** In the special case we explore, we define the following population parameters and estimators. At the outset, we define quantities with matrix notation to be consistent with the notation used in the remainder of the paper. Later on, we restrict our analysis to the  $p = 1$  case for simplicity:

- Fully-Iterated (Population) Parameter (Closed-Form): for  $\lambda_N$  such that  $\frac{1}{N}\lambda_N \rightarrow 0$ ,

$$\begin{aligned}\beta_N &= \mathbb{E}(\widetilde{\text{Var}}_N^{-1}(Y | X)[XX^T + \frac{1}{N}\lambda_N I_p])^{-1} \mathbb{E}(\widetilde{\text{Var}}_N^{-1}(Y | X)[XY]) \\ &\stackrel{N \rightarrow \infty}{\rightarrow} \beta^* = \mathbb{E}(\text{Var}^{-1}(Y | X)[XX^T])^{-1} \mathbb{E}(\text{Var}^{-1}(Y | X)[XY]) \\ &\equiv [\mathbb{E}(XX^T)]^{-1} \mathbb{E}(XY)\end{aligned}$$

- Fully-Iterated Estimator (Closed-Form):

$$\hat{\beta}_N^* = \mathbb{P}_N(\widetilde{\text{Var}}_N^{-1}(Y | X)[XX^T + \frac{1}{N}\lambda_N I_p])^{-1} \mathbb{P}_N(\widetilde{\text{Var}}_N^{-1}(Y | X)[XY])$$

- Unweighted Penalized (Initial Estimator) Population Parameter: if  $\frac{1}{N}\lambda_{0,N} \rightarrow 0$ ,

$$\beta_N^{(0)} = \mathbb{E}(XX^T + \frac{1}{N}\lambda_{0,N} I_p) \mathbb{E}(XY) \stackrel{N \rightarrow \infty}{\rightarrow} \beta^*$$

- Unweighted Penalized (Initial) Estimator:  $\hat{\beta}_N^{(0)} = \mathbb{P}_N(XX^T + \frac{1}{N}\lambda_{0,N} I_p) \mathbb{P}_N(XY)$

- Coefficient Estimator Variance:

$$\begin{aligned}
S_N(\beta) &= H_N^{-1}(\beta) M_N(\beta) H_N^{-1}(\beta) \\
&= \frac{1}{N} \{ \mathbb{E}[\widetilde{\text{Var}}_N^{-1}(Y | X) [XX^T + \frac{1}{N} \lambda_N I_p]] \}^{-1} \left[ \mathbb{E} \left( \frac{\text{Var}(Y | X)}{\widetilde{\text{Var}}_N^2(Y | X)} XX^T \right) + \right. \\
&\quad \left. \text{Var} \{ \widetilde{\text{Var}}_N^{-1}(Y | X) XX^T (\beta - \beta^*) \} \right] \{ \mathbb{E}[\widetilde{\text{Var}}_N^{-1}(Y | X) XX^T + \frac{1}{N} \lambda_N I_p] \}^{-1} \\
&\asymp \frac{1}{N} (\mathbb{E}[\text{Var}^{-1}(Y | X) XX^T])^{-1} \quad \text{as } N \rightarrow \infty \text{ (if } \beta \rightarrow \beta^*)
\end{aligned}$$

- Variance of Initial Coefficient Estimator

$$\begin{aligned}
S_N^{(0)}(\beta) &= \frac{1}{N} (\mathbb{E}[XX^T + \frac{1}{N} \lambda_{0,N} I_p])^{-1} \{ \mathbb{E}[\text{Var}(Y | X) XX^T] + \text{Var}[XX^T(\beta - \beta^*)] \} (\mathbb{E}[XX^T + \frac{1}{N} \lambda_{0,N} I_p])^{-1} \\
&\asymp \frac{1}{N} (\mathbb{E}[XX^T])^{-1} \{ \mathbb{E}[\text{Var}(Y | X) XX^T] \} (\mathbb{E}[XX^T])^{-1} \quad \text{as } N \rightarrow \infty \text{ (if } \beta \rightarrow \beta^*)
\end{aligned}$$

We now begin our exploration of this special case. First, observe that the above definitions imply, so long as  $\frac{1}{N} \lambda_N \rightarrow 0$  and  $\frac{1}{N} \lambda_{0,N} \rightarrow 0$ ,

$$S_N^{-1}(\beta_N) S_N^{(0)}(\beta_N^{(0)}) \xrightarrow{N \rightarrow \infty} \mathbb{E}[\text{Var}^{-1}(Y | X) XX^T] (\mathbb{E}[XX^T])^{-1} \mathbb{E}[\text{Var}(Y | X) XX^T] (\mathbb{E}[XX^T])^{-1},$$

so that  $S_N^{-1}(\beta_N) S_N^{(0)}(\beta_N^{(0)}) = O(1)$ .

Thus, when  $p = 1$ , the Taylor expansion for the quantity in condition (vi) has the form:

$$\begin{aligned}
S_N^{-1/2}(\beta_N) \left( \widehat{\beta}_{0,N} - \beta_N \right) &\stackrel{p \equiv 1}{=} \frac{\widehat{\beta}_N^{(0)} - \beta_N^{(0)}}{\sqrt{S_N(\beta_N)}} + \frac{\beta_N^{(0)} - \beta_N}{\sqrt{S_N(\beta_N)}} \\
&= O(1) * \underbrace{\frac{\widehat{\beta}_N^{(0)} - \beta_N^{(0)}}{\sqrt{S_N^{(0)}(\beta_N^{(0)})}}}_{\substack{\xrightarrow{d} N(0,1) \\ \text{under weak} \\ \text{CLT conditions}}} + A
\end{aligned}$$

where

$$A = \frac{\sqrt{N} \left\{ \mathbb{E} \left( \frac{X^2}{\tilde{\sigma}^2(X)} \right) + \frac{1}{N} \lambda_N \right\}}{\sqrt{\mathbb{E} \left( \frac{\sigma^2(X)}{\tilde{\sigma}^4(X)} X^2 \right) + (\beta_N - \beta^*) \text{Var} \left( \frac{X^2}{\tilde{\sigma}^2(X)} \right)}} * \frac{\frac{1}{N} \lambda_N \mathbb{E}(XY) \mathbb{E} \left( \frac{1}{\tilde{\sigma}^2(X)} \right) - \frac{1}{N} \lambda_{0,N} \mathbb{E}(XY / \tilde{\sigma}^2(X))}{\{\mathbb{E}(X^2) + \frac{1}{N} \lambda_{0,N}\} \left\{ \mathbb{E} \left( \frac{X^2}{\tilde{\sigma}^2(X)} \right) + \frac{1}{N} \lambda_N \mathbb{E} \left( \frac{1}{\tilde{\sigma}^2(X)} \right) \right\}}$$

$$= O(1) \quad \text{if } \frac{1}{N} \lambda_N = O(n^{-1/2}) \text{ and } \frac{1}{N} \lambda_{0,N} = O(n^{-1/2})$$

The above expansion shows that if, individually,  $\frac{1}{N} \lambda_N = O(N^{-1/2})$  and  $\frac{1}{N} \lambda_{0,N} = O(N^{-1/2})$ , then the initial (unweighted) estimator converges at the same rate to  $\beta_N$  as the fully-iterated (weighted) estimator. That is, in this special case, condition (vi) follows from the assumption that the scaled smoothing parameters of both estimators go to zero asymptotically at a rate of  $1/\sqrt{n}$  or faster.

## Appendix C Additional Simulation Experiments

### C.1 Additional Simulations: Gaussian AR1

We simulated data from the model

$$Y_{i,j}(s) = \beta_0(s) + X_{1,i} \beta_1(s) + X_{2,i,j} \beta_2(s) + \epsilon_{i,j}(s) \quad (14)$$

where  $\beta_0(s) = 3 + \sin(\pi s) + \sqrt{2} \cos(3\pi s)$ ,  $\beta_1(s) = 3 + \cos(2\pi s) + \sqrt{2} \cos(3\pi s)$ ,  $\beta_2(s) = 5\phi(\frac{s-0.35}{0.1}) - 5\phi(\frac{s-0.65}{0.2})$ ,  $s \in \mathcal{S} \equiv [0, 1]$ ,  $|\mathcal{S}| = 100$ , and  $\phi(\cdot)$  denotes the standard normal density function. Basing our simulations off of those in Li et al. (2022), we drew  $X_{1,i} \sim N(0, 1)$ , and  $X_{2,i,j} = j + e_{i,j}$ , where  $e_{i,j} \sim N(\alpha e_{i,j-1}, 1)$ , with  $e_{i,0} = 0$ ,  $\alpha = 0.7$ .

We first assess performance in simulations where the marginal covariance of the functional outcome has the structure adopted in our estimator: the  $S n_i \times S n_i$  covariance matrix  $\text{Cov}(\mathbf{Y}_i | \mathbb{X}_i) = \text{Cov}(\boldsymbol{\epsilon}_i) = \text{blockdiag}(\Sigma_i(1), \dots, \Sigma_i(S))$ , where  $\Sigma(s) = \text{Cov}(\mathbf{Y}_i(s) | \mathbb{X}_i) = \text{Cov}(\boldsymbol{\epsilon}_i(s)) \in \mathbb{R}^{n_i \times n_i}$ . We simulated data with the pointwise AR1 correlation structure  $\Sigma_{i,j}(s) = \sigma_\epsilon^2 \rho^{|i-j|}$  for all  $s \in \mathcal{S}$ . We set  $\sigma_\epsilon^2 = 10$  and  $\rho \in \{0.25, 0.5, 0.75\}$ .

We compared the One-Step to three benchmarks: 1) a penalized GLS with an independence working correlation structure (GLS-Ind), 2) a GLS with an exchangeable correlation structure

(GLS-Ex), and 3) the initial FoSR estimator,  $\hat{\beta}_{\Lambda_0}^{(0)}$  (fit with `pffr`). We constructed CIs using a sandwich estimator (Chen et al., 2013) for all methods, using the corresponding independence or exchangeable  $\mathbb{V}_i$  forms. We show in Appendix Table 20 that coverage is comparable between CIs constructed with sandwich and fast bootstrap variance estimators. Benchmark 1) shows how our implementation and tuning scheme performs without exploiting intra-cluster correlation, 2) shows performance of an estimator similar to a fully-iterated version of the One-Step fGEE (using the same exchangeable correlation structure), and 3) shows the performance of a FoSR that ignores intra-cluster correlation. CIs for the FoSR fit (benchmark 3) should, however, achieve nominal coverage in this correlated setting, given that we use a sandwich variance estimator.

Table 12 shows that the One-Step improves estimation performance compared to  $\hat{\theta}_{\Lambda_0}^{(0)}$  (FoSR) and the GLS-Ind. One-Step performance is comparable to that of the GLS-AR1, suggesting that it is asymptotically as efficient as the fully iterated GEE. Table 13 shows that the FoSR yields overly conservative pointwise and joint CIs, while the One-Step yields roughly nominal coverage, although inference is slightly anti-conservative when both  $N$  and  $n_i$  grow large. Coverage of the FoSR appears to also drop with large  $N$  and  $n_i$ . Table 14 shows that the FoSR yields overly conservative pointwise CIs, while the One-Step and GLS methods are a bit anti-conservative. All methods grow more anti-conservative as  $n_i$  grows. Table 15 shows that the One-Step is fast, taking only 2.5-3 minutes to fit on a dataset with  $N = 100$ , and  $n_i = 100$ , without parallelization.

Together these results suggest that 1) the One-Step improves estimation accuracy compared to working independence methods, 2) is as efficient as the fully iterated GEE (given similarity in performance to the GLS) in even moderate sample sizes, 3) is scalable to large cluster sizes and numbers, and 4) achieves approximately nominal coverage.

## C.2 Gaussian Exchangeable

Here we simulate data as in main text Section 4.2 “Simulation 2: Gaussian Outcome with Exchangeable Correlation,” except that we set  $\xi_{i,1} \stackrel{\text{iid}}{\sim} N(0, 5)$ ,  $\xi_{i,2} \stackrel{\text{iid}}{\sim} N(0, 2)$ ,  $\zeta_{i,j,1} \stackrel{\text{iid}}{\sim} N(0, 3)$  and  $\xi_{i,j,2} \stackrel{\text{iid}}{\sim} N(0, 1)$ .  $\epsilon_{i,j}(s) \stackrel{\text{iid}}{\sim} N(0, 10)$ . We set  $\sigma_\epsilon^2 = 10$ .



$N$	$n_i$	One-Step			GLS-AR1			GLS-Ind		
		0.25	0.5	0.75	0.25	0.5	0.75	0.25	0.5	0.75
25	5	0.99 $\pm$ 0.00	0.97 $\pm$ 0.00	0.93 $\pm$ 0.00	1.01 $\pm$ 0.00	0.98 $\pm$ 0.00	0.95 $\pm$ 0.00	1.00 $\pm$ 0.00	0.97 $\pm$ 0.00	0.94 $\pm$ 0.00
	25	0.96 $\pm$ 0.00	0.92 $\pm$ 0.00	0.85 $\pm$ 0.00	0.98 $\pm$ 0.00	0.93 $\pm$ 0.00	0.86 $\pm$ 0.00	0.98 $\pm$ 0.00	0.95 $\pm$ 0.00	0.91 $\pm$ 0.00
	100	0.97 $\pm$ 0.00	0.93 $\pm$ 0.00	0.87 $\pm$ 0.00	0.99 $\pm$ 0.00	0.95 $\pm$ 0.00	0.88 $\pm$ 0.00	1.00 $\pm$ 0.00	0.97 $\pm$ 0.00	0.93 $\pm$ 0.00
50	5	0.98 $\pm$ 0.00	0.96 $\pm$ 0.00	0.93 $\pm$ 0.00	0.99 $\pm$ 0.00	0.97 $\pm$ 0.00	0.93 $\pm$ 0.00	0.98 $\pm$ 0.00	0.96 $\pm$ 0.00	0.93 $\pm$ 0.00
	25	0.97 $\pm$ 0.00	0.93 $\pm$ 0.00	0.86 $\pm$ 0.00	0.97 $\pm$ 0.00	0.93 $\pm$ 0.00	0.86 $\pm$ 0.00	0.98 $\pm$ 0.00	0.95 $\pm$ 0.00	0.91 $\pm$ 0.00
	100	0.97 $\pm$ 0.00	0.94 $\pm$ 0.00	0.88 $\pm$ 0.00	0.98 $\pm$ 0.00	0.95 $\pm$ 0.00	0.89 $\pm$ 0.00	0.98 $\pm$ 0.00	0.97 $\pm$ 0.00	0.93 $\pm$ 0.00
100	5	0.97 $\pm$ 0.00	0.95 $\pm$ 0.00	0.93 $\pm$ 0.00	0.98 $\pm$ 0.00	0.96 $\pm$ 0.00	0.93 $\pm$ 0.00	0.97 $\pm$ 0.00	0.95 $\pm$ 0.00	0.93 $\pm$ 0.00
	25	0.96 $\pm$ 0.00	0.92 $\pm$ 0.00	0.86 $\pm$ 0.00	0.97 $\pm$ 0.00	0.93 $\pm$ 0.00	0.86 $\pm$ 0.00	0.97 $\pm$ 0.00	0.95 $\pm$ 0.00	0.91 $\pm$ 0.00
	100	0.97 $\pm$ 0.00	0.95 $\pm$ 0.00	0.90 $\pm$ 0.00	0.98 $\pm$ 0.00	0.95 $\pm$ 0.00	0.90 $\pm$ 0.00	0.99 $\pm$ 0.00	0.97 $\pm$ 0.00	0.94 $\pm$ 0.00

Table 12: Functional Coefficient Estimation Performance relative to initial FoSR fit, which assumes working independence correlation structure ( $\text{RMSE}_{AR1}/\text{RMSE}_{FoSR}$ ). Cells contain the average of 300 replicates  $\pm$  SEM (SEM= 0.00 indicates a value  $< 0.01$ ).

$N$	$n_i$	One-Step			GLS-AR1			GLS-Ind			FoSR		
		0.25	0.5	0.75	0.25	0.5	0.75	0.25	0.5	0.75	0.25	0.5	0.75
25	5	0.97 $\pm$ 0.00	0.97 $\pm$ 0.00	0.97 $\pm$ 0.00	0.97 $\pm$ 0.00	0.97 $\pm$ 0.00	0.97 $\pm$ 0.00	0.97 $\pm$ 0.00	0.97 $\pm$ 0.00	0.97 $\pm$ 0.00	1.00 $\pm$ 0.00	1.00 $\pm$ 0.00	1.00 $\pm$ 0.00
	25	0.97 $\pm$ 0.00	0.97 $\pm$ 0.00	0.97 $\pm$ 0.00	0.97 $\pm$ 0.00	0.97 $\pm$ 0.00	0.97 $\pm$ 0.00	0.97 $\pm$ 0.00	0.97 $\pm$ 0.00	0.97 $\pm$ 0.00	1.00 $\pm$ 0.00	1.00 $\pm$ 0.00	1.00 $\pm$ 0.00
	100	0.95 $\pm$ 0.00	0.95 $\pm$ 0.00	0.94 $\pm$ 0.00	0.95 $\pm$ 0.00	0.95 $\pm$ 0.00	0.94 $\pm$ 0.00	0.95 $\pm$ 0.00	0.96 $\pm$ 0.00	0.97 $\pm$ 0.00	0.98 $\pm$ 0.00	0.99 $\pm$ 0.00	0.99 $\pm$ 0.00
50	5	0.98 $\pm$ 0.00	0.98 $\pm$ 0.00	0.98 $\pm$ 0.00	0.98 $\pm$ 0.00	0.98 $\pm$ 0.00	0.98 $\pm$ 0.00	0.98 $\pm$ 0.00	0.98 $\pm$ 0.00	0.98 $\pm$ 0.00	1.00 $\pm$ 0.00	1.00 $\pm$ 0.00	1.00 $\pm$ 0.00
	25	0.97 $\pm$ 0.00	0.97 $\pm$ 0.00	0.97 $\pm$ 0.00	0.97 $\pm$ 0.00	0.97 $\pm$ 0.00	0.97 $\pm$ 0.00	0.97 $\pm$ 0.00	0.98 $\pm$ 0.00	0.98 $\pm$ 0.00	1.00 $\pm$ 0.00	1.00 $\pm$ 0.00	1.00 $\pm$ 0.00
	100	0.94 $\pm$ 0.00	0.94 $\pm$ 0.00	0.92 $\pm$ 0.00	0.94 $\pm$ 0.00	0.94 $\pm$ 0.00	0.92 $\pm$ 0.00	0.94 $\pm$ 0.00	0.96 $\pm$ 0.00	0.97 $\pm$ 0.00	0.97 $\pm$ 0.00	0.98 $\pm$ 0.00	0.98 $\pm$ 0.00
100	5	0.98 $\pm$ 0.00	0.99 $\pm$ 0.00	0.99 $\pm$ 0.00	0.99 $\pm$ 0.00	0.99 $\pm$ 0.00	0.99 $\pm$ 0.00	0.99 $\pm$ 0.00	0.99 $\pm$ 0.00	0.99 $\pm$ 0.00	1.00 $\pm$ 0.00	1.00 $\pm$ 0.00	1.00 $\pm$ 0.00
	25	0.96 $\pm$ 0.00	0.96 $\pm$ 0.00	0.96 $\pm$ 0.00	0.96 $\pm$ 0.00	0.97 $\pm$ 0.00	0.96 $\pm$ 0.00	0.97 $\pm$ 0.00	0.97 $\pm$ 0.00	0.98 $\pm$ 0.00	1.00 $\pm$ 0.00	1.00 $\pm$ 0.00	1.00 $\pm$ 0.00
	100	0.91 $\pm$ 0.00	0.92 $\pm$ 0.00	0.90 $\pm$ 0.00	0.91 $\pm$ 0.00	0.92 $\pm$ 0.00	0.90 $\pm$ 0.00	0.92 $\pm$ 0.00	0.94 $\pm$ 0.00	0.95 $\pm$ 0.00	0.93 $\pm$ 0.00	0.96 $\pm$ 0.00	0.97 $\pm$ 0.00

Table 13: Functional Coefficient Joint 95% Confidence Interval Coverage. Data are simulated with an AR1 correlation structure. Cells contain the average of 300 replicates  $\pm$  SEM (SEM= 0.00 indicates a value  $< 0.01$ ).

$N$	$n_i$	One-Step			GLS-AR1			GLS-Ind			FoSR		
		0.25	0.5	0.75	0.25	0.5	0.75	0.25	0.5	0.75	0.25	0.5	0.75
25	5	0.89 $\pm$ 0.00	0.89 $\pm$ 0.00	0.89 $\pm$ 0.00	0.90 $\pm$ 0.00	0.89 $\pm$ 0.00	0.89 $\pm$ 0.00	0.90 $\pm$ 0.00	0.89 $\pm$ 0.00	0.89 $\pm$ 0.00	0.99 $\pm$ 0.00	0.99 $\pm$ 0.00	0.99 $\pm$ 0.00
	25	0.89 $\pm$ 0.00	0.89 $\pm$ 0.00	0.88 $\pm$ 0.00	0.89 $\pm$ 0.00	0.89 $\pm$ 0.00	0.88 $\pm$ 0.00	0.89 $\pm$ 0.00	0.89 $\pm$ 0.00	0.89 $\pm$ 0.00	0.99 $\pm$ 0.00	0.99 $\pm$ 0.00	0.99 $\pm$ 0.00
	100	0.87 $\pm$ 0.00	0.87 $\pm$ 0.00	0.85 $\pm$ 0.00	0.86 $\pm$ 0.00	0.87 $\pm$ 0.00	0.85 $\pm$ 0.00	0.87 $\pm$ 0.00	0.88 $\pm$ 0.00	0.89 $\pm$ 0.00	0.96 $\pm$ 0.00	0.96 $\pm$ 0.00	0.95 $\pm$ 0.00
50	5	0.91 $\pm$ 0.00	0.91 $\pm$ 0.00	0.91 $\pm$ 0.00	0.91 $\pm$ 0.00	0.91 $\pm$ 0.00	0.91 $\pm$ 0.00	0.91 $\pm$ 0.00	0.91 $\pm$ 0.00	0.91 $\pm$ 0.00	0.99 $\pm$ 0.00	0.99 $\pm$ 0.00	0.99 $\pm$ 0.00
	25	0.90 $\pm$ 0.00	0.90 $\pm$ 0.00	0.89 $\pm$ 0.00	0.90 $\pm$ 0.00	0.90 $\pm$ 0.00	0.89 $\pm$ 0.00	0.90 $\pm$ 0.00	0.90 $\pm$ 0.00	0.91 $\pm$ 0.00	0.99 $\pm$ 0.00	0.99 $\pm$ 0.00	0.99 $\pm$ 0.00
	100	0.86 $\pm$ 0.00	0.86 $\pm$ 0.00	0.84 $\pm$ 0.00	0.86 $\pm$ 0.00	0.86 $\pm$ 0.00	0.84 $\pm$ 0.00	0.86 $\pm$ 0.00	0.88 $\pm$ 0.00	0.89 $\pm$ 0.00	0.93 $\pm$ 0.00	0.94 $\pm$ 0.00	0.95 $\pm$ 0.00
100	5	0.91 $\pm$ 0.00	0.92 $\pm$ 0.00	0.92 $\pm$ 0.00	0.92 $\pm$ 0.00	0.92 $\pm$ 0.00	0.92 $\pm$ 0.00	0.92 $\pm$ 0.00	0.92 $\pm$ 0.00	0.92 $\pm$ 0.00	0.99 $\pm$ 0.00	0.99 $\pm$ 0.00	0.99 $\pm$ 0.00
	25	0.89 $\pm$ 0.00	0.89 $\pm$ 0.00	0.88 $\pm$ 0.00	0.89 $\pm$ 0.00	0.89 $\pm$ 0.00	0.88 $\pm$ 0.00	0.89 $\pm$ 0.00	0.90 $\pm$ 0.00	0.91 $\pm$ 0.00	0.99 $\pm$ 0.00	0.99 $\pm$ 0.00	0.99 $\pm$ 0.00
	100	0.83 $\pm$ 0.00	0.84 $\pm$ 0.00	0.82 $\pm$ 0.00	0.84 $\pm$ 0.00	0.85 $\pm$ 0.00	0.83 $\pm$ 0.00	0.84 $\pm$ 0.00	0.86 $\pm$ 0.00	0.87 $\pm$ 0.00	0.89 $\pm$ 0.00	0.91 $\pm$ 0.00	0.94 $\pm$ 0.00

Table 14: Functional Coefficient Pointwise 95% Confidence Interval Coverage. Data are simulated with an AR1 correlation structure. Cells contain the average of 300 replicates  $\pm$  SEM (SEM= 0.00 indicates a value  $< 0.01$ ).

Table 16 shows the estimation performance and illustrates that the One-Step performs comparably to the GLS-Ex, suggesting the One-Step performs comparably to a fully-iterated GEE. Moreover the One-Step performs comparably to the marginal approach (Li et al., 2022) that models correlation across the functional domain (both within- and across longitudinal observations of the functional outcome). Thus, in these simulations, modeling correlation at each point  $s$ , is enough to capture efficiency gains. Table 18 shows that the pointwise coverage of the One-Step is often close to the nominal levels. In contrast, the Marginal approach is often highly anti-conservative for large  $n_i$ , a quality acknowledged in (Li et al., 2022). The GLS approaches

$N$	$n_i$	One-Step			GLS-AR1			GLS-Ind			FoSR		
		0.25	0.5	0.75	0.25	0.5	0.75	0.25	0.5	0.75	0.25	0.5	0.75
25	5	16.54 ± 0.10	16.21 ± 0.07	24.79 ± 0.18	8.35 ± 0.04	8.20 ± 0.02	12.08 ± 0.01	9.69 ± 0.05	9.55 ± 0.04	12.26 ± 0.02	0.15 ± 0.00	0.15 ± 0.00	0.22 ± 0.00
	25	22.56 ± 0.15	20.80 ± 0.12	20.47 ± 0.11	12.28 ± 0.10	11.55 ± 0.08	11.13 ± 0.05	12.52 ± 0.11	11.78 ± 0.09	11.23 ± 0.07	0.28 ± 0.00	0.27 ± 0.00	0.26 ± 0.00
	100	45.85 ± 0.58	39.32 ± 0.17	41.68 ± 0.50	34.17 ± 0.50	29.34 ± 0.31	28.54 ± 0.27	30.27 ± 0.46	26.13 ± 0.22	26.24 ± 0.27	1.05 ± 0.02	0.72 ± 0.00	0.73 ± 0.01
50	5	24.18 ± 0.15	22.93 ± 0.14	23.26 ± 0.06	14.60 ± 0.09	14.44 ± 0.08	14.16 ± 0.03	16.29 ± 0.09	16.22 ± 0.10	16.21 ± 0.08	0.22 ± 0.00	0.21 ± 0.00	0.21 ± 0.00
	25	33.37 ± 0.22	32.74 ± 0.28	33.42 ± 0.25	21.95 ± 0.24	21.54 ± 0.15	22.68 ± 0.25	21.62 ± 0.19	21.32 ± 0.13	22.30 ± 0.20	0.48 ± 0.00	0.48 ± 0.00	0.49 ± 0.00
	100	82.80 ± 1.03	84.35 ± 1.11	86.85 ± 1.19	61.59 ± 0.72	69.19 ± 1.03	68.34 ± 1.02	53.39 ± 0.65	60.84 ± 0.92	59.75 ± 0.90	1.54 ± 0.02	1.79 ± 0.03	1.66 ± 0.03
100	5	37.37 ± 0.13	36.62 ± 0.12	37.55 ± 0.13	26.49 ± 0.09	26.45 ± 0.08	26.23 ± 0.07	27.42 ± 0.11	28.07 ± 0.16	27.67 ± 0.13	0.30 ± 0.00	0.31 ± 0.00	0.30 ± 0.00
	25	62.10 ± 0.80	70.89 ± 0.20	57.45 ± 0.47	46.39 ± 0.48	59.69 ± 0.61	46.66 ± 0.57	42.84 ± 0.30	52.79 ± 0.25	41.42 ± 0.40	0.77 ± 0.00	1.24 ± 0.00	0.76 ± 0.00
	100	187.81 ± 3.17	175.73 ± 2.32	176.43 ± 2.67	159.26 ± 2.62	161.64 ± 2.81	144.59 ± 2.33	131.43 ± 5.45	122.23 ± 1.69	114.57 ± 1.50	3.17 ± 0.08	4.16 ± 0.09	3.09 ± 0.04

Table 15: Fit Time (seconds) for the entire One-Step estimation procedure including 1) estimating the initial  $\hat{\beta}_{\Lambda_0}^{(0)}$ , 2) estimating correlation parameters, 3) tuning  $\Lambda_1$ , 4) calculating the One-Step  $\hat{\beta}_{\Lambda_1}^{(1)}$ , and 5) estimating  $\widehat{\text{Var}}(\hat{\beta}_{\Lambda_1}^{(1)})$  and constructing CIs. Data are simulated with an AR1 correlation structure. Cells contain the average of 300 replicates  $\pm$  SEM (SEM= 0.00 indicates a value  $< 0.01$ ).

$N$	$n_i$	One-Step	GLS-Ex	GLS-Ind	Marginal
25	5	0.96 ± 0.00	0.96 ± 0.00	1.00 ± 0.00	0.96 ± 0.01
	25	0.97 ± 0.00	0.97 ± 0.00	1.00 ± 0.00	0.99 ± 0.01
	100	1.00 ± 0.00	1.00 ± 0.00	1.00 ± 0.00	1.01 ± 0.01
50	5	0.95 ± 0.01	0.95 ± 0.01	0.99 ± 0.00	0.95 ± 0.01
	25	0.97 ± 0.00	0.97 ± 0.00	1.00 ± 0.00	0.98 ± 0.01
	100	0.99 ± 0.00	0.99 ± 0.00	1.00 ± 0.00	1.02 ± 0.01
100	5	0.95 ± 0.01	0.95 ± 0.00	0.99 ± 0.00	0.94 ± 0.01
	25	0.97 ± 0.00	0.97 ± 0.00	1.00 ± 0.00	0.97 ± 0.01
	100	0.99 ± 0.00	0.99 ± 0.00	1.00 ± 0.00	—

Table 16: Gaussian Exchangeable: RMSE relative to the relative to the initial FoSR fit  $\hat{\theta}_{\Lambda_0}^{(0)}$  (fit with `pffr()`). We indicate out-of-memory (30Gb) with the symbol —. Cells contain the average of 300 replicates  $\pm$  SEM (SEM= 0.00 indicates a value  $< 0.01$ ).

are often highly conservative, while the FoSR is slightly more anti-conservative compared to the One-Step in smaller samples. Table 17 shows that the joint coverage tends to be slightly more conservative than the FoSR, but both are substantially less conservative than the GLS approaches.

$N$	$n_i$	One-Step	GLS-Ex	GLS-Ind	FoSR
25	5	$0.97 \pm 0.00$	$1.00 \pm 0.00$	$1.00 \pm 0.00$	$0.95 \pm 0.01$
	25	$0.97 \pm 0.00$	$1.00 \pm 0.00$	$1.00 \pm 0.00$	$0.97 \pm 0.00$
	100	$0.98 \pm 0.00$	$1.00 \pm 0.00$	$1.00 \pm 0.00$	$0.97 \pm 0.00$
50	5	$0.99 \pm 0.00$	$1.00 \pm 0.00$	$1.00 \pm 0.00$	$0.95 \pm 0.01$
	25	$0.99 \pm 0.00$	$1.00 \pm 0.00$	$1.00 \pm 0.00$	$0.98 \pm 0.00$
	100	$0.98 \pm 0.00$	$1.00 \pm 0.00$	$1.00 \pm 0.00$	$0.98 \pm 0.00$
100	5	$0.99 \pm 0.00$	$1.00 \pm 0.00$	$1.00 \pm 0.00$	$0.96 \pm 0.00$
	25	$0.99 \pm 0.00$	$1.00 \pm 0.00$	$1.00 \pm 0.00$	$0.99 \pm 0.00$
	100	$0.99 \pm 0.00$	$1.00 \pm 0.00$	$1.00 \pm 0.00$	$0.98 \pm 0.00$

Table 17: Gaussian Exchangeable: Joint 95% CI coverage. Cells contain the average of 300 replicates  $\pm$  SEM (SEM= 0.00 indicates a value  $< 0.01$ ).

$N$	$n_i$	One-Step	GLS-Ex	GLS-Ind	Marginal	FoSR
25	5	$0.92 \pm 0.00$	$0.96 \pm 0.00$	$0.96 \pm 0.00$	$0.94 \pm 0.00$	$0.90 \pm 0.00$
	25	$0.92 \pm 0.00$	$0.95 \pm 0.00$	$0.96 \pm 0.00$	$0.94 \pm 0.00$	$0.92 \pm 0.00$
	100	$0.94 \pm 0.00$	$0.97 \pm 0.00$	$0.96 \pm 0.00$	$0.71 \pm 0.00$	$0.93 \pm 0.00$
50	5	$0.95 \pm 0.00$	$0.97 \pm 0.00$	$0.97 \pm 0.00$	$0.94 \pm 0.00$	$0.91 \pm 0.00$
	25	$0.95 \pm 0.00$	$0.97 \pm 0.00$	$0.97 \pm 0.00$	$0.95 \pm 0.00$	$0.94 \pm 0.00$
	100	$0.94 \pm 0.00$	$0.96 \pm 0.00$	$0.97 \pm 0.00$	$0.70 \pm 0.00$	$0.93 \pm 0.00$
100	5	$0.96 \pm 0.00$	$0.98 \pm 0.00$	$0.97 \pm 0.00$	$0.95 \pm 0.00$	$0.92 \pm 0.00$
	25	$0.96 \pm 0.00$	$0.98 \pm 0.00$	$0.98 \pm 0.00$	$0.95 \pm 0.00$	$0.94 \pm 0.00$
	100	$0.96 \pm 0.00$	$0.97 \pm 0.00$	$0.98 \pm 0.00$	—	$0.95 \pm 0.00$

Table 18: Gaussian Exchangeable: Pointwise CI coverage. We indicate out-of-memory (30Gb) with the symbol —. Cells contain the average of 300 replicates  $\pm$  SEM (SEM= 0.00 indicates a value  $< 0.01$ ).

$N$	$n_i$	One-Step	GLS-Ex	GLS-Ind	Marginal	FoSR
25	5	$20.66 \pm 0.14$	$9.05 \pm 0.07$	$8.05 \pm 0.04$	$0.49 \pm 0.00$	$0.16 \pm 0.00$
	25	$23.24 \pm 0.10$	$11.98 \pm 0.04$	$11.99 \pm 0.05$	$4.85 \pm 0.03$	$0.27 \pm 0.00$
	100	$54.87 \pm 0.59$	$35.85 \pm 0.55$	$35.03 \pm 0.54$	$75.15 \pm 1.07$	$1.17 \pm 0.01$
50	5	$27.45 \pm 0.18$	$16.00 \pm 0.13$	$14.60 \pm 0.11$	$1.15 \pm 0.01$	$0.21 \pm 0.00$
	25	$34.59 \pm 0.14$	$21.37 \pm 0.10$	$19.97 \pm 0.13$	$29.79 \pm 0.27$	$0.45 \pm 0.00$
	100	$86.76 \pm 1.05$	$64.70 \pm 0.51$	$66.35 \pm 0.63$	$415.64 \pm 2.57$	$2.15 \pm 0.01$
100	5	$39.33 \pm 0.21$	$27.26 \pm 0.13$	$26.51 \pm 0.14$	$3.79 \pm 0.03$	$0.31 \pm 0.00$
	25	$73.25 \pm 0.90$	$54.20 \pm 0.73$	$51.83 \pm 0.74$	$233.72 \pm 1.69$	$1.08 \pm 0.02$
	100	$146.26 \pm 2.27$	$102.88 \pm 1.43$	$87.89 \pm 0.99$	—	$2.79 \pm 0.01$

Table 19: Gaussian Exchangeable: Time to fit. We indicate out-of-memory (30Gb) with the symbol —. Cells contain the average of 300 replicates  $\pm$  SEM (SEM= 0.00 indicates a value  $< 0.01$ ).

### C.3 Comparison of Variance Estimators

Here we compare the performance of different strategies to estimate coefficient estimator variance and construct pointwise confidence intervals. The results below are from the simulation experiments described in main text Section 4.1, “Simulation 2: Gaussian Outcome with Exchangeable Correlation.”

Table 20 shows that pointwise CIs constructed using  $\widehat{\text{Var}}\left(\widehat{\boldsymbol{\theta}}_{\Lambda_1}^{(1)}\right)$ , estimated with the sandwich or fast cluster bootstrap, achieve comparable coverage. This suggests that the fast cluster bootstrap accurately estimates  $\widehat{\text{Var}}\left(\widehat{\boldsymbol{\theta}}_{\Lambda_1}^{(1)}\right)$  and can be used instead of the sandwich estimator.

Table 21 shows that the sandwich and fast cluster bootstrap strategies take comparable time as both require inversion of one  $p \times p$  matrix. Taken together the sandwich estimator and fast cluster bootstrap yield comparable estimation accuracy and take comparable amounts of time.

$N$	$n_i$	Fast Bootstrap	Sandwich
25	5	$0.92 \pm 0.01$	$0.93 \pm 0.01$
	25	$0.92 \pm 0.01$	$0.93 \pm 0.01$
	100	$0.94 \pm 0.01$	$0.95 \pm 0.00$
50	5	$0.94 \pm 0.01$	$0.95 \pm 0.00$
	25	$0.95 \pm 0.00$	$0.95 \pm 0.00$
	100	$0.94 \pm 0.01$	$0.94 \pm 0.01$
100	5	$0.95 \pm 0.00$	$0.96 \pm 0.00$
	25	$0.96 \pm 0.00$	$0.96 \pm 0.00$
	100	$0.95 \pm 0.00$	$0.96 \pm 0.00$

Table 20: Pointwise CIs, constructed using  $\widehat{\text{Var}}\left(\widehat{\boldsymbol{\theta}}_{\Lambda_1}^{(1)}\right)$  estimated with the sandwich or the fast cluster bootstrap, achieve comparable coverage. These results are from the Gaussian Exchangeable data simulations from main text Section 4.1. This shows that the fast cluster bootstrap performs well as an estimator for  $\text{Var}\left(\widehat{\boldsymbol{\theta}}_{\Lambda_1}^{(1)}\right)$  and can be used as an alternative to the sandwich estimator. Cells contain the average of 300 replicates  $\pm$  SEM (SEM= 0.00 indicates a value  $< 0.01$ ).

$N$	$n_i$	Fast Bootstrap	Sandwich
25	5	$19.63 \pm 0.20$	$17.66 \pm 0.08$
	25	$25.86 \pm 0.23$	$24.63 \pm 0.15$
	100	$44.96 \pm 0.19$	$40.60 \pm 0.42$
50	5	$25.69 \pm 0.10$	$25.77 \pm 0.10$
	25	$39.01 \pm 0.33$	$34.75 \pm 0.30$
	100	$77.62 \pm 0.45$	$82.05 \pm 1.04$
100	5	$37.52 \pm 0.14$	$37.78 \pm 0.14$
	25	$57.95 \pm 0.34$	$58.95 \pm 0.46$
	100	$147.34 \pm 1.32$	$151.24 \pm 3.15$

Table 21: Total time of fitting the One-Step (sec), including tuning  $\Lambda_1$ , and estimating  $\text{Var}(\widehat{\boldsymbol{\theta}}_{\Lambda_1}^{(1)})$ , when using sandwich and fast cluster bootstrap variance estimators. The differences in the timing between columns are thus entirely determined by variance estimators,  $\text{Var}(\widehat{\boldsymbol{\theta}}_{\Lambda_1}^{(1)})$ . The relative speed of the sandwich and the fast cluster bootstrap depend on  $N$  and  $n_i$ , but are mostly comparable. This shows that the fast cluster bootstrap can be used as an alternative to the sandwich estimator. Cells contain the average of 300 replicates  $\pm$  SEM.

## C.4 Comparison of Joint CIs constructed with Parametric and Non-Parametric Bootstrap Based Strategies

Here we present the coverage of joint CIs constructed with a non-parametric bootstrap based strategy. This approach is based on Section “BUILDING SIMULTANEOUS CONFIDENCE BANDS” in (Degras, 2017). However, we estimate the empirical quantile used to construct CIs in terms of resampling  $\widehat{\boldsymbol{\theta}}^{(1)}$  instead of  $\widehat{\boldsymbol{\beta}}^{(1)}$ . The joint CI coverage of the non-parametric cluster bootstrap-based approach is similar to the coverage achieved by the parametric bootstrap-based strategy for joint CI construction, presented in main text 3. This shows that the non-parametric cluster bootstrap-based approach can also be used to construct joint CIs. We emphasize that the non-parametric bootstrap strategy explored here calculates  $\tilde{q}_{1-\alpha}^{(r)}$  using a non-parametric bootstrap. It is distinct from an approach that simply estimates  $\text{Var}(\widehat{\boldsymbol{\theta}}_{\Lambda_1}^{(1)})$  with a non-parametric cluster bootstrap and then calculates the empirical quantile of the joint CI,  $\tilde{q}_{1-\alpha}^{(r)}$ , using a parametric bootstrap.

$N$	$n_i$	Non-Parametric
25	5	$0.97 \pm 0.00$
	25	$0.97 \pm 0.00$
	100	$0.98 \pm 0.00$
50	5	$0.99 \pm 0.00$
	25	$0.99 \pm 0.00$
	100	$0.98 \pm 0.00$
100	5	$0.99 \pm 0.00$
	25	$0.99 \pm 0.00$

Table 22: Joint 95% CI Coverage for joint CIs constructed with a non-parametric cluster bootstrap-based approach. These results are from the Gaussian Exchangeable data simulations from main text Section 4.1. Cells contain the average of 300 replicates  $\pm$  SEM (SEM= 0.00 indicates a value  $< 0.01$ ).

## Appendix D Additional Application Analyses

### D.1 Whisker Activity

Since the authors were interested in how cells from this brain region encoded the sensory input of whisker activity, they recorded how much the whiskers moved when they were experimentally manipulated. The movement-by-moment activity of the whiskers can thus be used as a functional covariate to estimate how the association evolves across time. We fit the following concurrent model

$$\text{logit}(\mathbb{P}[Y_{i,j,l}(s) \mid X_{i,j}(s)]) = \beta_0(s) + X_{i,j}(s)\beta_1(s),$$

where  $X_{i,j}(s) \in \mathbb{R}$  is a measurement of whisker activity at trial timepoint  $s$  on trial  $j$  for the animal that neuron  $i$  was recorded from. We centered and scaled whisker activity for interpretability.

Because  $\widehat{\beta}_1(s)$  is significantly positive throughout the entire trial (i.e. across the functional domain), suggests that the neuron-whisker association is not driven by whisker stimulation. Interestingly the magnitude of association is roughly twice as high with the AR1 structure. Both the intercept and the functional slope suggest that the whisker stimulation (occurring at timepoint 0 sec) has only a small influence on the association between neural activity and whisker activity. Since  $X_{i,j}(s)$  is centered and scaled, the functional intercept can be interpreted as the mean log odds of neural activity at an average speed. This appears to be affected by the stimulation as the shape of the functional intercept appears to rapidly increase and then decrease after stimulation (timepoint 0 sec). The AR1 analysis, for example, took 13.5min, illustrating its speed for large datasets with functional covariates.

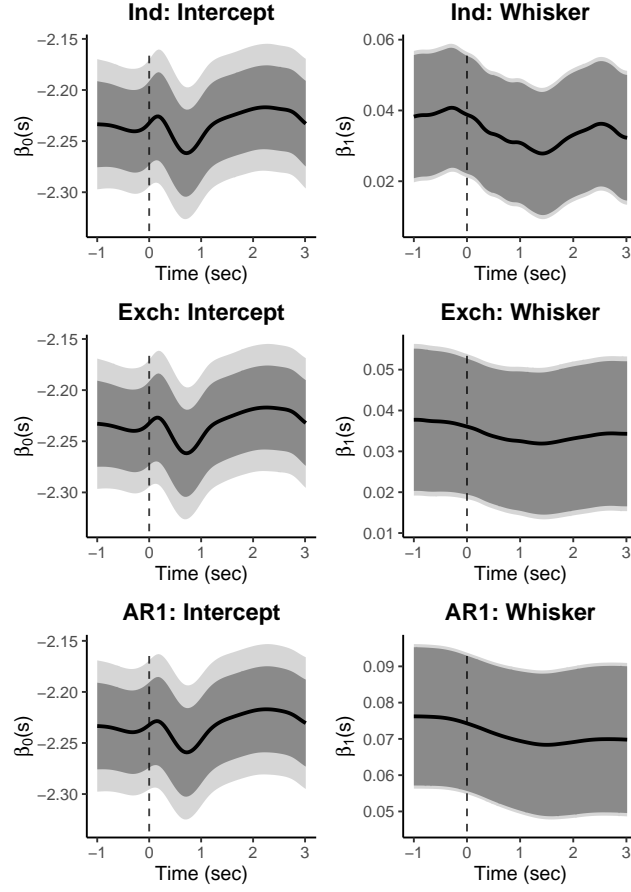


Figure 2: **Whisker-Neural activity association.** Functional coefficient estimates for Independent (Ind), Exchangeable (Exch), and Auto-regressive-1 (AR1) working correlation structures. Time relative to whisker stimulation.



## References

- Allévius, B. (2018). On the precision matrix of an irregularly sampled ar(1) process.
- Ammar, G. S. and Gragg, W. B. (1988). Superfast solution of real positive definite toeplitz systems. *SIAM Journal on Matrix Analysis and Applications*, 9(1):61–76.
- Barrett, T., Dowle, M., Srinivasan, A., Gorecki, J., Chirico, M., Hocking, T., Schwendinger, B., and Krylov, I. (2025). *data.table: Extension of ‘data.frame’*. R package version 1.17.99, <https://Rdatatable.gitlab.io/data.table>, <https://github.com/Rdatatable/data.table>.
- Brockhaus, S., Scheipl, F., Hothorn, T., and Greven, S. (2015). The functional linear array model. *Statistical Modelling*, 15(3):279–300.
- Chen, H., Wang, Y., Paik, M. C., and Choi, H. A. (2013). A marginal approach to reduced-rank penalized spline smoothing with application to multilevel functional data. *Journal of the American Statistical Association*, 108(504):1216–1229.
- Cheng, G., Yu, Z., and Huang, J. Z. (2013). The cluster bootstrap consistency in generalized estimating equations. *Journal of Multivariate Analysis*, 115:33–47.
- Coddington, L. T., Lindo, S. E., and Dudman, J. T. (2023). Mesolimbic dopamine adapts the rate of learning from action. *Nature*, 614(7947):294–302.
- Crainiceanu, C. M., Goldsmith, J., Leroux, A., and Cui, E. (2024). *Functional data analysis with R*. CRC Press.
- Cui, E., Leroux, A., Smirnova, E., and Crainiceanu, C. M. (2022). Fast univariate inference for longitudinal functional models. *Journal of Computational and Graphical Statistics*, 31(1):219–230.
- Degras, D. (2017). Simultaneous confidence bands for the mean of functional data. *WIREs Computational Statistics*, 9(3):e1397.
- Eckardt, M., Mateu, J., and Greven, S. (2024). Generalized functional additive mixed models with (functional) compositional covariates for areal covid-19 incidence curves. *Journal of the Royal Statistical Society Series C: Applied Statistics*, 73(4):880–901.
- Glaser, J., Whiteway, M., Cunningham, J. P., Paninski, L., and Linderman, S. (2020). Recurrent switching dynamical systems models for multiple interacting neural populations. In Larochelle, H., Ranzato, M., Hadsell, R., Balcan, M., and Lin, H., editors, *Advances in Neural Information Processing Systems*, volume 33, pages 14867–14878. Curran Associates, Inc.
- Goldsmith, J., Scheipl, F., Huang, L., Wrobel, J., Di, C., Gellar, J., Harezlak, J., McLean, M. W., Swihart, B., Xiao, L., Crainiceanu, C., Reiss, P. T., and Cui, E. (2024). *refund regression with functional data*. R package version 0.1-37.
- Greven, S., Crainiceanu, C., Caffo, B., and Reich, D. (2011). Longitudinal functional principal component analysis. In *Recent advances in functional data analysis and related topics*, pages 149–154. Springer.
- Grienberger, C., Giovannucci, A., Zeiger, W., and Portera-Cailliau, C. (2022). Two-photon calcium imaging of neuronal activity. *Nature Reviews Methods Primers*, 2(1):67.

- Guha Niyogi, P. and Zhong, P.-S. (2025). Quadratic inference with dense functional responses. *Journal of Multivariate Analysis*, 207:105400.
- Guo, W. (2002). Functional mixed effects models. *Biometrics*, 58(1):121–128.
- Inácio, A. R., Lam, K. C., Zhao, Y., Pereira, F., Gerfen, C. R., and Lee, S. (2025). Brain-wide presynaptic networks of functionally distinct cortical neurons. *Nature*.
- Jeong, H., Taylor, A., Floeder, J. R., Lohmann, M., Mihalas, S., Wu, B., Zhou, M., Burke, D. A., and Namboodiri, V. M. K. (2022). Mesolimbic dopamine release conveys causal associations. *Science*, 378(6626):eabq6740.
- Jewell, S. and Witten, D. (2018). Exact spike train inference via l0 optimization. *The annals of applied statistics*, 12(4):2457.
- Jun, J. J., Steinmetz, N. A., Siegle, J. H., Denman, D. J., Bauza, M., Barbarits, B., Lee, A. K., Anastassiou, C. A., Andrei, A., Aydın, Ç., Barbic, M., Blanche, T. J., Bonin, V., Couto, J., Dutta, B., Gratiy, S. L., Gutnisky, D. A., Häusser, M., Karsh, B., Ledochowitsch, P., Lopez, C. M., Mitelut, C., Musa, S., Okun, M., Pachitariu, M., Putzeys, J., Rich, P. D., Rossant, C., Sun, W.-l., Svoboda, K., Carandini, M., Harris, K. D., Koch, C., O’Keefe, J., and Harris, T. D. (2017). Fully integrated silicon probes for high-density recording of neural activity. *Nature*, 551(7679):232–236.
- Kuschnig, N. (2023). *sanic: Solving  $Ax = b$  Nimbly in C++*. R package version 0.0.2.
- Legaria, A. A., Matikainen-Ankney, B. A., Yang, B., Ahanonu, B., Licholai, J. A., Parker, J. G., and Kravitz, A. V. (2022). Fiber photometry in striatum reflects primarily nonsomatic changes in calcium. *Nature Neuroscience*, 25(9):1124–1128.
- Li, R., Xiao, L., Smirnova, E., Cui, E., Leroux, A., and Crainiceanu, C. M. (2022). Fixed-effects inference and tests of correlation for longitudinal functional data. *Statistics in Medicine*, 41(17):3349–3364.
- Liang, K.-Y. and Zeger, S. L. (1986). Longitudinal data analysis using generalized linear models. *Biometrika*, 73(1):13–22.
- Ling, Y. and Lysy, M. (2022). *SuperGauss: Superfast Likelihood Inference for Stationary Gaussian Time Series*. R package version 2.0.3.
- Lipsitz, S., Fitzmaurice, G., Sinha, D., Hevelone, N., Hu, J., and Nguyen, L. L. (2017). One-step generalized estimating equations with large cluster sizes. *Journal of Computational and Graphical Statistics*, 26(3):734–737.
- Loewinger, G., Cui, E., Lovinger, D., and Pereira, F. (2025). A statistical framework for analysis of trial-level temporal dynamics in fiber photometry experiments. *Elife*, 13:RP95802.
- Molenberghs, G., Verbeke, G., et al. (2005). Models for discrete longitudinal data.
- Morris, J. S. and Carroll, R. J. (2006). Wavelet-based functional mixed models. *Journal of the Royal Statistical Society Series B: Statistical Methodology*, 68(2):179–199.
- Papadakis, M., Tsagris, M., Dimitriadis, M., Fafalios, S., Tsamardinos, I., Fasiolo, M., Borboudakis, G., Burkardt, J., Zou, C., and Lakiotaki, K. (2018). Package ‘rfast’.

- Pnevmatikakis, E. A., Soudry, D., Gao, Y., Machado, T. A., Merel, J., Pfau, D., Reardon, T., Mu, Y., Lacefield, C., Yang, W., et al. (2016). Simultaneous denoising, deconvolution, and demixing of calcium imaging data. *Neuron*, 89(2):285–299.
- Qu, A. and Li, R. (2005). Quadratic inference functions for varying-coefficient models with longitudinal data. *Biometrics*, 62(2):379–391.
- Roesch, M. R., Singh, T., Brown, P. L., Mullins, S. E., and Schoenbaum, G. (2009). Ventral striatal neurons encode the value of the chosen action in rats deciding between differently delayed or sized rewards. *Journal of Neuroscience*, 29(42):13365–13376.
- Scheipl, F., Gertheiss, J., and Greven, S. (2016). Generalized functional additive mixed models. *Electronic Journal of Statistics*.
- Scheipl, F., Staicu, A.-M., and Greven, S. (2015). Functional additive mixed models. *Journal of Computational and Graphical Statistics*, 24(2):477–501.
- Sergazinov, R., Leroux, A., Cui, E., Crainiceanu, C., Aurora, R. N., Punjabi, N. M., and Gaynanova, I. (2023). A case study of glucose levels during sleep using multilevel fast function on scalar regression inference. *Biometrics*, 79(4):3873–3882.
- Shou, H., Zipunnikov, V., Crainiceanu, C. M., and Greven, S. (2015). Structured functional principal component analysis. *Biometrics*, 71(1):247–257.
- Touloumis, A. (2016). Simulating correlated binary and multinomial responses under marginal model specification: The simcormultres package. *The R Journal*, 8:79–91. <https://rjournal.github.io/>.
- Venables, W. N. and Ripley, B. D. (2002). *Modern Applied Statistics with S*. Springer, New York, fourth edition. ISBN 0-387-95457-0.
- Walker, G. T. (1931). On periodicity in series of related terms. *Proceedings of the Royal Society of London. Series A, Containing Papers of a Mathematical and Physical Character*, 131(818):518–532.
- Wang, X., Kolar, M., and and, A. S. (2025). Statistical inference for networks of high-dimensional point processes. *Journal of the American Statistical Association*, 120(550):1014–1024.
- Willmore, L., Minerva, A. R., Engelhard, B., Murugan, M., McMannon, B., Oak, N., Thiberge, S. Y., Peña, C. J., and Witten, I. B. (2023). Overlapping representations of food and social stimuli in mouse vta dopamine neurons. *Neuron*, 111(22):3541–3553.e8.
- Wood, S. N. (2011). Fast stable restricted maximum likelihood and marginal likelihood estimation of semiparametric generalized linear models. *Journal of the Royal Statistical Society Series B: Statistical Methodology*, 73(1):3–36.
- Wood, S. N. (2017). *Generalized Additive Models: An Introduction with R*. Chapman and Hall/CRC, 2 edition.
- Xia, L. and Shojaie, A. (2024). Inference for linear functionals of high-dimensional longitudinal proteomics data using generalized estimating equations.

- Yule, G. U. (1927). Vii. on a method of investigating periodicities disturbed series, with special reference to wolfer’s sunspot numbers. *Philosophical Transactions of the Royal Society of London. Series A, Containing Papers of a Mathematical or Physical Character*, 226(636-646):267–298.
- Zhang, Y., Rózsa, M., Liang, Y., Bushey, D., Wei, Z., Zheng, J., Reep, D., Broussard, G. J., Tsang, A., Tsegaye, G., Narayan, S., Obara, C. J., Lim, J.-X., Patel, R., Zhang, R., Ahrens, M. B., Turner, G. C., Wang, S. S. H., Korff, W. L., Schreier, E. R., Svoboda, K., Hasseman, J. P., Kolb, I., and Looger, L. L. (2023). Fast and sensitive gcamp calcium indicators for imaging neural populations. *Nature*, 615(7954):884–891.
- Zhou, X., Cui, E., Sartini, J., and Crainiceanu, C. (2025). Prediction inference using generalized functional mixed effects models. *arXiv preprint arXiv:2501.07842*.
- Zhu, H., Chen, K., Luo, X., Yuan, Y., and Wang, J.-L. (2019). Fmem: Functional mixed effects models for longitudinal functional responses. *Statistica Sinica*, 29(4):2007.
- Zipunnikov, V., Greven, S., Shou, H., Caffo, B., Reich, D. S., and Crainiceanu, C. (2014). Longitudinal high-dimensional principal components analysis with application to diffusion tensor imaging of multiple sclerosis. *The annals of applied statistics*, 8(4):2175.